Symbiosis-related genes sustain the development of a downy mildew pathogen on *Arabidopsis thaliana*

Martina K. Ried[1, #,§], Aline Banhara[1,#], Andreas Binder[1], Fang-Yu Hwu[1], Andrea A. Gust[2], Caroline Höfle[3], Ralph Hückelhoven[3], Thorsten Nürnberger[2], and Martin Parniske[1,*]

[1] University of Munich (LMU), Faculty of Biology, Genetics, Großhaderner Str. 2-4, 82152 Martinsried, Germany

[2] University of Tübingen, Center for Plant Molecular Biology, Plant Biochemistry, Auf der Morgenstelle 32, 72076 Tübingen, Germany

[3] Technische Universität München, Center of Life and Food Sciences Weihenstephan, Emil-Ramann-Str. 2, 85350, Freising-Weihenstephan, Germany

[#] Authors contributed equally

[*] Correspondence: Martin Parniske; e-mail: parniske@lmu.de; Phone: +49 (0)89 / 2180-74700; Fax: +49 (0)89 / 2180-74702

[§] present address: University of Geneva, Structural Plant Biology Laboratory, Department of Botany and Plant Biology, 30 Quai Ernest Ansermet, 1211 Geneva, Switzerland

ABSTRACT

The interfaces through which nutrients are transferred from plant cells to arbuscular mycorrhiza fungi and biotrophic hyphal pathogens are structurally similar. We report that in *Arabidopsis thaliana*, mutations in homologs of common symbiosis genes (CSGs) encoding homologs of the symbiosis receptor kinase SYMRK, the nucleoporins NUP133 and SEC13 or the cation channel POLLUX reduce the reproductive success of *Hyaloperonospora arabidopsidis (Hpa).* Analysis of the multiplication of extracellular bacterial pathogens, *Hpa*-induced cell death or callose accumulation, as well as *Hpa*- or flg22-induced defence marker gene expression, did not reveal any traces of constitutive or exacerbated defence responses. We discovered an age-dependent, possibly senescence-related transition of haustorial shape that occurred significantly earlier and at higher frequency in the CSG mutants. These findings point to a function of the homologs of common symbiosis genes in haustorial maintenance thus revealing an overlapping gene set for the intracellular accommodation of hyphal symbionts and pathogens.

INTRODUCTION

Most land plant species feed carbon sources to arbuscular mycorrhiza (AM) fungi, which in turn deliver phosphate and other nutrients via finely branched intracellular structures called arbuscules

(Gutjahr and Parniske, 2013, Gutjahr, 2014). The accommodation of fungal symbionts inside living plant cells involves substantial developmental reprogramming of the host plant cell, initiated by the formation of the pre-penetration apparatus, a transvacuolar cytoplasmic bridge formed in anticipation of fungal infection (Genre et al., 2005, Genre et al., 2008). The oomycetal downy mildew pathogen *Hyaloperonospora arabidopsidis* (*Hpa*) develops intracellular feeding organs, so called haustoria, which exhibit structural similarities to the arbuscules of AM fungi. Like arbuscules, haustoria are accommodated inside plant cells and are entirely surrounded by a plant-derived membrane, which keeps the pathogen physically outside the host cytoplasm (Mims et al., 2002, Pumplin and Harrison, 2009, Hückelhoven and Panstruga, 2011). Structural and functional similarities between accommodation structures for intracellular microbes raised the hypothesis that the corresponding symbiotic and pathogenic associations rely on a shared genetic program (Parniske, 2000). This would imply that filamentous hyphal pathogens exploit an Achilles heel, the presence of the symbiotic program in most land plant species, for their own parasitic lifestyle (Parniske, 2000, Evangelisti et al., 2014).

In the present study, we tested this hypothesis by focussing on an ancient genetic program comprising the *common symbiosis genes* (CSGs), which is conserved among angiosperms for the intracellular accommodation of AM fungi (Stracke et al., 2002, Endre et al., 2002, Imaizumi-Anruko et al., 2004, Ané et al., 2004, Levy et al., 2004, Mitra et al., 2004, Kistner et al., 2005, Saito et al., 2007, Yano et al., 2008, Banba et al., 2008, Groth et al., 2010). In legumes and Actinorhiza host plants, the CSGs are also required for root nodule symbiosis (RNS) with nitrogen-fixing rhizobia or Frankia bacteria, respectively (Kistner et al., 2005, Markmann et al., 2008, Gherbi et al., 2008, Svistoonoff et al., 2013). In the legume *Lotus japonicus*, the products of some of the CSGs - the malectin-like domain leucine-rich repeat receptor-like kinase (MLD-LRR-RLK) Symbiosis Receptor-like Kinase SYMRK (Stracke et al., 2002, Markmann et al., 2008, Antolin-Llovera et al., 2014, Ried et al., 2014), the nucleoporins NUP85, NUP133 and SEC13 homolog (SEH1) of the NUP107-160 subcomplex (Kanamori et al., 2006, Alber et al., 2007, Saito et al., 2007, Groth et al., 2010), as well as the nuclear-envelope localised cation channel POLLUX (Charpentier et al., 2008, Venkateshwaran et al., 2012) - are implicated in a signal transduction pathway leading from the perception of microbial signalling molecules at the plasma membrane to the induction of calcium oscillations in and around the nucleus (calcium-spiking), which finally results in the activation of symbiosis-related genes and a developmental reprogramming of the respective host cells (Gutjahr and Parniske, 2013, Oldroyd, 2013).

Arabidopsis thaliana belongs to the Brassicaceae, a plant lineage that lost the ability to establish AM symbiosis after the divergence of the Brassicales (Favre et al., 2014, Delaux et al., 2014, Bravo et al.,

2016). This asymbiotic state correlates with the loss of specific CSGs encoding e.g. the nuclear calcium-spiking decoder complex consisting of the calcium and calmodulin-depended protein kinase CCaMK and its phosphorylation target CYCLOPS, which is of central importance for transcriptional regulation in symbioses (Singh and Parniske, 2012, Singh et al., 2014, Favre et al., 2014, Bravo et al., 2016, Pimprikar et al., 2016, Cerri et al., 2017). These findings suggest a strong selection for the genome-wide loss of symbiosis-related genes. *A. thaliana* can, however, establish a compatible interaction with *Hpa,* and besides the loss of certain CSGs, retained homologs of other CSGs in its genome. The retention of these CSGs in the *A. thaliana* genome, as well as the striking similarities between arbuscules and haustoria led us to investigate whether this vestigial symbiotic gene set plays a role in the interaction of *A. thaliana* with *Hpa,* the fungal powdery mildew pathogen *Erysiphe cruciferarum*, which forms intracellular haustoria in *A. thaliana* epidermal leaf cells, or the extracellular bacterial pathogen *Pseudomonas syringae*.

RESULTS

We inspected the *A. thaliana* genome for the presence of CSGs and identified candidate orthologs of *POLLUX* and of nucleoporin genes of the NUP107-160 subcomplex (Figure 1 – Figure Supplement 1 + 2). Even though a direct ortholog of *SYMRK* has been deleted from the *A. thaliana* genome (Kevei et al., 2005), the products of two *A. thaliana* genes, which we consequently named *SYMRK-homologous Receptor-like Kinase* 1 (*ShRK1*) and *ShRK2,* were identified as the close relatives of *LjSYMRK* ((Markmann et al., 2008); Figure 1- Figure Supplement 1 - 4).

Lines carrying insertional mutant alleles of these CSGs were analysed for their phenotype in the interaction with *Hpa*. In *pollux*, *shrk1*, *shrk2*, the *shrk1* x *shrk2* double mutant, as well as a reference line with a T-DNA insertion in *Phytosulfokine Receptor 1* (*pskr1)* (Matsubayashi et al., 2006, Mosher et al., 2013) or a references line with an EMS-induced mutation in *Constitutive expression of PR genes 5* (*cpr5*) (Bowling et al., 1997), the reproductive success of *Hpa* isolate NoCo2 - measured as sporangiophore number per cotyledon or spore production - was significantly reduced compared to wild-type plants (Figure 1 a + c; Figure 1 – Figure Supplement 5).

To capture potential structural or functional shifts during evolution, we included a range of NUP107-160 subcomplex members in our analysis that exceeded the list previously described as functionally relevant in the root symbioses of *L. japonicus*. The *sec13* and *nup133* single mutants and the *sec13* x *nup133* double mutant impaired *Hpa* reproductive success (Figure 1 a + c; Figure 1 – Figure Supplement 5), while lines with T-DNA insertions in *nup43*, *nup85*, *nup160* and *seh1* did not (Figure 1 b).

The reduced *Hpa* reproductive success could not be explained by a decreased frequency of haustoria formation measured as percentage of host cells contacted by hyphae that harbour an haustorium. Other than a slight decrease in *pollux*, the frequency in the other mutants was indistinguishable from the wild-type (Figure 1 – Figure Supplement 6).

However, all *A. thaliana* CSG mutants but not *nup43*, *nup85*, *nup160* and *seh1* mutants exhibited a significant shift in the ratio of haustoria morphologies (Figure 2; Figure 2 – Figure Supplement 3). At 5 days post infection (dpi) the majority of haustoria in leaves of the wild-type had a globular, single-lobed appearance. Deviations from such morphology, typically characterised by multiple lobes on a single haustorium ("multilobed"), were observed as well. The amount of multilobed haustoria in the CSG mutants was significantly increased, a phenomenon that was alleviated in the tested complementation lines (Figure 2 a + b; Figure 2 – Figure Supplement 1). Overexpression of *L. japonicus SYMRK* in the *shrk1 x shrk2* double mutant resulted in a significant reduction of multilobed haustoria (Figure 2 a). In contrast to the CSG mutants, the disease resistant *pskr1* mutant did not show any signs of altered haustoria development (Figure 2 a). In both, wild-type and *shrk1* x *shrk2*, the percentage of multilobed haustoria increased over time, but was significantly higher in *shrk1* x *shrk2* at each analysed time point (Figure 2 d). To visualise the perihaustorial membrane *in vivo*, we made use of stable transgenic *A. thaliana* lines either expressing the N-terminally YFP-tagged remorin AtREM1.2 (At3g61260) under the control of its native promoter (*pAt3g61260:YFP-At3g61260* (Jarsch et al., 2014)) or RPW8.2:YFP (Wang et. al., 2009) (Figure 2 – Figure Supplement 3 c + 4). We could confirm that multi-lobed haustoria appeared already in living plant cells and observed that the loss of YFP-AtREM1.2 fluorescence was associated with changes in haustoria morphology; while 49 - 68 % of the single-lobed haustoria exhibited YFP-AtREM1.2 fluorescence, only 14 – 19 % of the multi-lobed haustoria contained detectable amounts of YFP-AtREM1.2 at their perihaustorial membrane (Figure 2 – Figure Supplement 4).

L. japonicus SYMRK belongs to the LRR I-RLK family of receptor kinases, which consists of 50 members in *A. thaliana* (Shiu and Bleecker, 2003, Hok et al., 2011). Despite the large number of such RLKs in the *A. thaliana* genome, a detailed phenotypic analysis has only been published for Impaired Oomycete Susceptibility 1 (IOS1), which is involved in defence-related signalling (Chen et al., 2014, Hok et al., 2011). On the one hand, *IOS1* supports the infection of an obligate biotrophic oomycetal pathogen, but on the other hand, is important for the resistance against bacteria (Chen et al., 2014, Hok et al., 2011). Interestingly, we could only observe altered haustoria morphology in an *ios1* mutant of the *A. thaliana* ecotype Ler but not in an *ios1* mutant of Col-0, which might imply that different paralogs are important for plant-microbe interaction in different ecotypes (Figure 2 – Figure Supplement 2).

To investigate the specificity of the role of CSGs in plant-pathogen interactions, we infected the CSG mutants with the haustoria-forming powdery mildew fungus *E. cruciferarum*. We did not observe a consistent reduction in the reproductive success of *E. cruciferarum* (Figure 1 – Figure Supplement 7). A morphological comparison of haustoria shape was not attempted because of the much more complex and highly variable haustoria morphology in this interaction.

Plant evolution resulted in several strategies to defend themselves against microbial pathogens. For example, PAMP triggered immunity (PTI) is triggered by the perception of pathogen-associated molecular patterns (PAMPs) or plant-derived damage-associated molecular patterns (DAMPs) and results in plant defence responses accompanied by the activation of defence marker genes or callose deposition (Jones and Dangl, 2006; Antolin-Llovera et al., 2012; Gust et al., 2017). To analyse whether the increased *Hpa* resistance of the CSG mutants is a result of deregulated defence responses, we investigated the basal transcript levels of the three PAMP-induced marker genes - *Pathogenesis-Related gene 1* (*PR1*), a marker gene for salicylic acid (SA)-mediated resistance (Ryals et al., 1996), *Ethylene Response Factor 1* (*ERF1*), a marker gene for ethylene-mediated resistance (Solano et al., 1998) and the plant defensin *PDF1.2a*, a marker gene for jasmonic acid (JA)- and ethylene-mediated resistance (Penninckx et al., 1996) in the absence of pathogenic attack. Transcript levels in the tested mutants under non-challenged conditions did not differ from transcript levels in the wild-type (Figure 3 a, black circles). To examine whether CSG mutants show exacerbated activation of defence marker genes, we analysed the transcript levels of *PR1*, *ERF1* and *PDF1.2a* in plants infected with *Hpa.* All tested genes were upregulated to a similar extend in the CSG mutants and the wild-type (Figure 3 a, empty circles). Only *PDF1.2a* transcript levels were significantly lower in *Hpa*-infected *shrk1 x shrk2* plants than in infected wild-type plants, however, it is unlikely that this is the reason for the increased pathogen resistance of the double mutant. Moreover, the ability of *Hpa* to suppress callose deposition around the haustorial neck region (Sohn et al., 2007) was not disturbed in the CSG mutants compared to the wild-type (Figure 3 b).

In addition to the expression levels of defence marker genes, we investigated other symptoms typically associated with deregulated immune responses. We could not observe any developmental or growth defects, which are typically a result of the hyper-activation of the SA-dependent defence pathway (Bowling et al., 1997), in CSG mutants grown side-by-side with the wild-type and the dwarf mutant *suppressor of npr1-1, constitutive 1* (*snc1* (Li et al., 2001)) (Figure 3 – Figure Supplement 1). Furthermore, we analysed constitutive and *Hpa*-induced hypersensitive response (HR) in CSG mutants and the wild-type (Figure 3 – Figure Supplement 2). Most of the non-infected leaves did not display any sign of cell death (Figure 3 – Figure Supplement 2; first column), but dark-blue stained dead cells were sporadically observed with no significant differences between non-infected leaves of

both wild-type and CSG mutants (Figure 3 – Figure Supplement 2; second column and upper graph). In infected leaves of the CSG mutants, cell death is detected in, or adjacent to, haustoria-containing cells in a frequency indistinguishable from or even lower than the wild-type (Figure 3 – Figure Supplement 2; third column and lower graph). In all genotypes, infected leaves contain hyphal strands growing in the absence of any cell death (Figure 3 – Figure Supplement 2; fourth column).

To examine whether mutations in CSGs have an effect on signalling related to PAMP-triggered immunity, we inspected the transcript levels of *Flg22-induced Receptor-like Kinase 1* (*FRK1* (Asai et al., 2002)) and *ERF1* in the wild-type, the CSG mutants and a *fls2* mutant (Figure 4 a) in response to the bacterial flagellin-derived peptide flg22 (Chinchilla et al., 2006). Transcript levels in mock-treated samples were not different in the wild-type and the analysed mutants, except for the *shrk1* mutant that displayed a slight increase in basal *FRK1* transcript levels, which was not detectable in the *shrk1 x shrk2* double mutant, and the *nup133 x sec13* double mutants that contained slightly decreased basal levels of *ERF1* transcripts. The deviations observed for individual mutants are unlikely responsible for the increased *Hpa* resistance. Six hours after flg22 treatment the tested genes were all upregulated to the same extend in the CSG mutants and the wild-type (Figure 4 a). Furthermore, we investigated the growth behaviour of *P. syringae* on the wild-type and on CSG mutants (Figure 4 b). *P. syringae* pv. *tomato* (*Pto*) DC3000 induces the activation of SA-dependent defence signalling in the host, and deregulation of this pathways impairs *P. syringae* resistance (Glazebrook, 2005). The growth of *Pto* DC3000 wild-type or the avirulent *ΔAvrPto/PtoB* strain was unaltered on the *A. thaliana* CSG mutants, providing further evidence that they do not exhibit constitutive or enhanced activation of SA-dependent defences (Figure 4 b).

DISCUSSION

Biotrophic hyphal pathogens depend on the vitality of their host cell for their own survival and reproduction because they frequently form intracellular feeding structures called haustoria. The developmental programs of the host that are supporting intracellular accommodation of haustoria are largely unexplored. Moreover, plant genes that are involved in the subcellular reprogramming of the host required for haustoria formation are largely unknown. Here we explored the hypothesis that the biotrophic pathogen *Hpa* exploits an ancestral pathway - defined by the so called common symbiosis genes (CSG) - that enabled intracellular accommodation in the context of arbuscular mycorrhiza and the nitrogen-fixing root nodule symbiosis.

CSG mutants reveal a link between the timing of haustorial shape shifts and reproductive success

We observed - based on sporangiophore and spore counts - that *A. thaliana* CSG mutants are impaired in supporting the reproduction of the oomycetal pathogen *Hpa*. This was associated with a shift in the haustoria morphology. While the frequency of multilobed haustoria increased in the wild-type as well as in the mutants over time, it was significantly higher in the *A. thaliana* CSG mutants at all time points analysed. This finding reveals a connection between haustoria morphology and the age of the interaction and suggests that haustoria aging is accelerated in the CSG mutants. It remains unclear whether single-lobed haustoria develop into multilobed haustoria over time, or whether in older interactions multilobed haustoria form directly, without a single lobed intermediate step. The presence of REM1.2 at the peri-haustorial membrane was strongly decreased around multilobed haustoria, indicating an age-related alteration of the protein composition of the perihaustorial membrane. It has been postulated that haustoria are the main avenue for nutrient acquisition from the host (Voegele, R. T. and Mendgen, K., 2003). Senescence of haustoria is associated with encasement and thus is likely to reduce their functionality (Caillaud et al., 2014). Therefore, it is likely that the premature formation of multilobed haustoria might be directly responsible for the reduction in *Hpa* reproductive success. Taken together our results suggest a role of Arabidopsis CSG genes in maintaining the single lobed, and presumably functional, stage of *Hpa* haustoria.

CSG mutants exhibit no traces of altered plant defence responses or regulation

In order to determine whether plant defence responses caused the reduction of the *Hpa* reproductive success, we quantified a range of defence symptoms in the wild-type and the mutants. Based on these analyses, we could rule out a constitutively or exacerbated activation of PTI signature marker genes. Furthermore, we did not detect an increased frequency of cell death, a symptom of defence-related hypersensitive responses. This is in accordance with the identical bacterial density reached in CSG mutants and the wild type. In summary, based on the analysis of a wide range of defence symptoms in the classical PTI assays and three different pathosystems, we conclude that *A. thaliana* CSG mutants display unaltered levels and frequencies of defence responses. Consequentially, the impairment of the *Hpa* interaction is not due to deregulated defence in these mutants.

Arabidopsis CSG mutants are specifically impaired in the *Hpa* interaction

We were unable to detect differences in the interaction of *A. thaliana* CSG mutants with the haustoria-forming powdery mildew fungus *E. cruciferarum* in comparison to wild-type plants. This may be due to the different cell types targeted by *Hpa* and *E. cruciferarum* for haustoria formation. *Hpa* infects the epidermal cells and then progresses to the mesophyll (Slusarenko and Schlaich, 2003) in which the vast majority of haustoria are formed, while *E. cruciferarum* forms haustoria directly within

epidermal cells (Micali et al., 2008). Cell-type specific functionality has been described for the CSGs under study (Hayashi et al., 2014, Bensmihen et al., 2011). In addition, the genetic requirements for the intracellular accommodation of fungal and oomycetal pathogens may differ. The *A. thaliana Mildew resistance Locus O* (*MLO)* gene, for instance, is an epidermal compatibility factor required for powdery mildew fungus penetration (Consonni et al., 2006), with no role in the *Hpa* interaction reported to date. However, it should be noted that the haustoria of *E. cruciferarum* are structurally very complex and irregularly shaped. Because of this inherent polymorphy, it is possible that we missed subtle structural changes caused by the CSG mutations.

Functional conservation of *common symbiosis gene* homologs between *A. thaliana* and *L. japonicus*

Intriguingly, transgenic complementation of a symbiosis-defective legume mutant with versions of the *A. thaliana* homolog of *POLLUX* indicates overall functional conservation (Venkateshwaran et al., 2012).

Likewise, successful restoration of the *Hpa* haustoria development in the *A. thaliana shrk1 x shrk* 2 double mutant by the legume *SYMRK* gene (Figure 2 a) indicates conservation of this functional feature despite loss of the actual *SYMRK* ortholog in the *A. thaliana* genome.

Despite of the critical cellular function of the nuclear pore complex for import and export, legume mutants defective in certain members of the nucleoporin subcomplex 107-160 are specifically defective in symbiosis with rhizobia and AM fungi, but otherwise largely free of macroscopically detectable phenotypes. We could confirm that also in *A. thaliana*, the overall size, shape and development of NUP107-160 complex mutants are macroscopically wild-type-like (Figure 3 – Figure Supplement 1). Several nucleoporins of the NUP107-160 subcomplex show a high rate of evolution (Bapteste et al., 2005), share similar structures and are therefore potentially able to replace each other, potentially allowing for distinct functional adaptations while keeping the overall complex structure intact (Binder and Parniske, 2013b). Agreeing with this, phenotypes of individual NUP107-160 subcomplex mutants vary both in occurrence and severity depending on the organism (Gonzalez-Aguilera and Askjaer, 2012, Binder and Parniske, 2013a). To capture potential structural or functional evolutionary shifts, we included more NUP107-160 subcomplex members than those previously described as functionally relevant for legume root symbioses. Interestingly, we found that the *sec13* and *nup133* single mutants and the *sec13* x *nup133* double mutant are impaired in the interaction with *Hpa*, while the *nup43*, *nup85*, *nup160* and *seh1* single mutants are not. This pattern is not 100% congruent with the observation in the legume *L. japonicus*, in which *seh1*, *nup85* and *nup133* impaired symbiosis (Kanamori et al., 2006, Saito et al., 2007, Groth et al., 2010), however, it clearly

sheds light on a specific role of this subcomplex for the root symbioses of legumes and the *Hpa* interaction of *A. thaliana*. The differences in the specific subcomplex members that reveal a phenotype may be explained by clade-specific adaptations of the NUP107-160 subcomplex. Furthermore, the NUP107-160 subcomplex has been implicated in plant defence; mutations in *NUP96*, *NUP160* and *SEH1* impair basal and resistance-gene mediated immunity (Zhang and Li, 2005, Wiermer et al., 2012). However, *A. thaliana* CSG nucleoporin mutants did not show such deregulation (Figure 3 + 4), possibly due to distinct roles of individual subcomplex components in compatibility and defence.

Genetic overlaps between symbiotic and pathogen biotrophic interactions

It is a long-standing hypothesis that plant pathogens exploit genetic pathways for the intracellular accommodation of mutualistic symbionts such as AM fungi or nitrogen-fixing bacteria (Parniske et al., 2000). Supporting this hypothesis, it has been reported that several genetic components important for mutualistic plant-microbe interactions are as well supporting the interaction of plant roots and filamentous pathogens (Wang et al., 2012, Rey et al., 2013, Rey et al., 2014).

The glycerol-phosphate acyl-transferase gene *RAM2* for example, is important for the successful colonisation of *Medicago truncatula* by the oomycetal pathogen *Phytophthora palmivora*, but it also plays a role in the development of AM fungal hyphopodia and arbuscules during AM symbiosis (Wang et al., 2012). This observation implies that a compatibility factor can be exploited by microbial pathogens and, likewise, by beneficial symbionts. In contrast to our findings, in the *ram2* mutant, the interaction with *P. palmivora* was already impaired at the stage of appressoria formation (Wang et al., 2012).

In the present study, we were able to demonstrate genetic commonalities of symbiosis and disease in the formation and maintenance of intracellular accommodation structures at a later developmental stage of the plant-microbe association. Although strongly suggested by the function of the CSGs, it remains unclear whether their *A. thaliana* homologs are similarly involved in a signal transduction pathway directly supporting oomycetal development. It will be therefore interesting to identify the mechanistic commonalities between symbiotic and pathogenic interactions that are controlled by the CSGs.

Loss of AM but retention of CSGs

The loss of AM symbiosis in *A. thaliana* and in four other independent plant lineages was correlated with the absence of more than 100 genes with potential roles in AM (Delaux et al., 2013, Favre et al., 2014, Delaux et al., 2014, Bravo et al., 2016). The requirement of CSGs for full *Hpa* reproductive success indicates that, like in *ram2*, pathogens exploit the ancient symbiotic program, and the

selection pressure resulting from this scenario provides a plausible explanation for the observed convergent pattern of symbiosis-related gene loss.

Hpa, a secret mutualist?

While the exploitation of symbiotic programs by pathogens might explain the consistent deletion of CSGs from five independent plant lineages, it raises the question, which evolutionary forces retained certain CSGs in an otherwise AM-asymbiotic plant. A housekeeping function was not revealed since no pleiotropic developmental phenotypes were observed in the mutants. This leaves us with the unexpected finding that the only detected role for the CSGs in *A. thaliana* is the support of an oomycete. It will be interesting to find out whether ecological conditions exist, under which oomycetal colonization might provide a selective advantage to the host plant (Salvaudon et al., 2008).

METHODS

Seed sterilization and plant growth

All *A. thaliana* mutants described in the manuscript were of Col-0 ecotype, except for *ios1*, which was either of Col-0 or Ler ecotype. Seeds were obtained from "The Nottingham Arabidopsis Stock Centre" – NASC (Scholl et al., 2000) or the GABI-DUPLO double mutant collection (Bolle et al., 2013). For *in vitro* experiments, *A. thaliana* seeds were sterilized by incubation for 5 min in sterilisation solution (70 % ethanol, 0.05 % Tween20), followed by incubation for 2 min in 100 % ethanol. For *Hpa* infection, seeds were directly germinated in soil and grown for two weeks under long day conditions (16 h light, 22 °C, 85 µmol m^{-2} s^{-1}). For *E. cruciferarum* inoculation, plants were grown in a 2:1 soil/sand mixture. Seeds were stratified for 48 h at 4 °C prior to transfer into a growth chamber (10 h light, 120 µmol m^{-2} s^{-1} light, 22 °C day, 20 °C night, 65% relative humidity). For elicitor treatment, seeds were placed on half-strength MS plates (Murashige and Skoog, 1962), stratified for 48 h at 4 °C in the dark, and grown for 8 days under long day conditions (16 h light, 23 °C, 85 µmol m^{-2} s^{-1}).

A. thaliana stable transformation

To transform *A. thaliana*, flowers were dipped in *Agrobacterium* suspensions as described previously (Clough and Bent, 1998).

Pathogen assays and phenotypic analyses

Seven days after infection, *A. thaliana* wild-type (Col-0 or Ler) leaves with sporulating *Hpa* isolate NoCo2 or *Hpa* isolate Waco9, respectively, were harvested into 15 mL reaction tubes containing 10 mL dH_2O and vortexed for 2 s. The spore solution was then filtered through a Miracloth filter and sprayed onto 12-days-old plants using a spraying device. Subsequently, plants were placed into trays

and covered with wet translucid lids. Trays were sealed to maintain high humidity, and plants were grown under long day conditions (16 h light, 18 °C, 85 µmol $m^{-2}s^{-1}$).

For spore counting, *A. thaliana* wild-type (Col-0) and mutant seedlings were harvested five days after infection. Ten seedlings per background were harvested into reaction tubes containing 1 mL dH_2O and vortexed for 3 min. The spore solution was then filtered through a Miracloth filter and spores were counted with a Fuchs Rosenthal chamber.

Cotyledons or leaves were harvested and stained in 0.01 % trypan-blue-lactophenol (10 mL lactic acid, 10 mL glycerol, 10 g phenol, 10 mg trypan blue dissolved in 10 mL distilled water) for 3 min at 95°C and 5 h at room temperature, followed by overnight clearing in saturated chloral hydrate (2.5 g/mL). For observation using differential interference contrast microscopy, samples were mounted in glycerol. For sporangiophore counting, a minimum of 50 cotyledons per genotype and replicate were analysed and the number of sporangiophores per infected cotyledon was plotted. For investigation of haustoria shape and penetration efficiency, a minimum of five leaves per genotype and replicate were analysed. On each leaf, the percentage of multilobed haustoria per total haustoria or the percentage of haustoria-containing cells per cells contacted by hyphae was calculated for 10 individual strands of hyphae. The mean for each leaf was calculated and plotted.

E. cruciferarum was grown on *A. thaliana* wild-type (Col-0) to maintain aggressiveness and on susceptible *phytoalexin deficient 4* (*pad4*) mutants (Glazebrook et al., 1996) for elevated conidia production. Plants were placed under a polyamide net (0.2 mm^2) and inoculated at a density of 3 – 4 conidia mm^{-2}, by brushing conidia off of *pad4* mutant leaves through the net. Two leaves per plant were harvested, cleared and kept in acetic acid (25 %) until microscopic analysis. Leaves were stained in acetic acid (25 %) ink (1:9) (Königsblau, Pelikan, 4001), washed in water, placed in water containing a few drops of Tween20, washed in water again, and analysed under a bright-field microscope. For each replicate, conidiophores per colony were counted on 10 colonies per leaf, on 5 - 10 leaves per genotype.

Bacterial strains *Pto* DC3000 or *Pto* DC3000 *ΔAvrPto/AvrPto* were grown and used for infection assays on leaves of 4 – 5 weeks old *A. thaliana* plants as described previously (Lin and Martin, 2005, Kemmerling et al., 2007).

Each experiment was performed at least three times independently.

Observation of haustoria

For morphology analysis of haustoria, leaves of *A. thaliana* wild-type (Col-0) or the *shrk1* x *shrk2* double mutant were harvested at 5 dpi, cleared in 10 M KOH for 5 min, stained with 0.05 % aniline blue in 0.067 M K_2HPO_4 for 20 min and observed with a confocal light scanning microscope (Leica

SP5; excitation at 360-380 nm, detection at 470-505 nm). Images were edited using ImageJ with the "volume viewer" plugin (Schneider et al., 2012).

For the Technovit section, leaves of *A. thaliana* wild-type (Col-0) or CSG mutants were infected with *Hpa* as described above and harvested at 7 dpi. Leaves were fixed by 3.7% formaldehyde and followed by a serial dehydration process by incubating samples in 30%, 50%, 70% and 100% ethanol. Samples were than incubated in the mixture of Technovit 7100 solution A (100 ml Technovit 7100, 1 pack Hardener 1, 2.5 ml PEG 4000) with ethanol in different proportion (solution A: 100% ethanol= 1:3, solution A: 100% ethanol= 1:1 and solution A: 100% ethanol= 3:1 each for 30 min, followed by solution A overnight). After the incubation, samples were mounted in the polymerization solution (15 ml solution A, 1 ml Hardener II) then held by the mount holders (10 ml Technovit 3040 and 5 ml universal liquid). Sections were made by LEICA RM2125RT for 7 μm thick. Technovit sections were than stained with 0.01 % trypan-blue-lactophenol solution, which described above, at 37 ^{o}C for at least 3 hr, until the sections turned blue. Then distained samples gently with a drop of chloral hydrate (2.5 g/mL) and rinsed by water. Technovit sections were observed under LEICA DMI 6000B microscope.

For quantification of fluorescence associated with the perihaustorial membrane, *A. thaliana* wild-type (Col-0) plants transformed with the construct *pAt3g61260:YFP-At3g61260* were infected with *Hpa* as described above, harvested at 8 dpi and observed with a microscope using differential interference contrast or epifluorescence microscopy with YFP filter settings (Leica DMI6000B; excitation at 500/20, emission at 535/30). The quantification was performed in triplicates. For each biological replicate consisting of 6 leaves, 100 single-lobed and 100 multilobed haustoria were counted and scored for detectable fluorescence. Haustoria without detectable fluorescence were visualized by differential interference contrast microscopy and scored as non-fluorescent.

A. thaliana wild-type (Col-0) plants expressing RPW8.2:YFP (Wang et. al., 2009) were infected with *Hpa* as described above, harvested at 10 dpi and observed with a confocal microscope with an Argon 488-nm laser exciter (Leica TCS SP5 confocal; excitation at 520, emission at 560) under ×63 NA 1.2 water-immersion lenses (Carl Zeiss Inc., Thornwood, NY, U.S.A.).

Analysis of oomycete-associated callose deposition

Oomycete-associated callose deposition was analysed on cotyledons of *A. thaliana* wild-type (Col-0) or CSG mutants. Leaves were harvested at 4 dpi, cleared in 10 M KOH for 5 min, stained with 0.05 % aniline blue in 0.067 M K_2HPO_4 for 20 min and mounted in glycerol for observation with an epifluorescence microscope with CFP filter settings (Leica DMI6000B; excitation 436/10, emission 465/30). Regions of interest (ROIs) covering the neck bands were selected in ImageJ(Schneider et

al., 2012) and the signal intensity of each neck band was calculated from single ROIs and mean intensities were plotted. n = 27 – 72.

Elicitor treatment

For pre-incubation, 8 days old seedlings were transferred to a 12-well plate (3 seedlings/well represent one biological replicate) with half-strength liquid MS medium (Murashige and Skoog, 1962) supplemented with 1 % sucrose and incubated overnight under long-day conditions (16 h light, 22 °C, 100 µmol m^{-2} s^{-1}; 8 h dark, 18 °C) and 100 rpm shaking. On the following day the medium was exchanged, half of the samples were supplemented with 1 µM flg22, and the other half was kept in half-strength MS to serve as mock controls. Plants were then incubated for 6 h at 22 °C and 100 rpm shaking. For every genotype, three biological replicates of treated and non-treated samples were harvested and immediately frozen in liquid N_2 for subsequent RNA extraction.

RNA Extraction and qPCR analysis

RNA extraction was performed using the Spectrum™ Plant Total RNA kit (Sigma-Aldrich), followed by DNase I treatment (amplification grade DNase I, Invitrogen™) to remove genomic DNA. First strand cDNA synthesis was performed from 250 ng total RNA using the SuperScript® III First-Strand Synthesis SuperMix (Invitrogen™) with oligo(dT) primers. qPCR was performed in 20 µL reactions containing 1x SYBR Green I (Invitrogen™) in a CFX96 Real-time PCR detection system (Bio-Rad). PCR program: 2’-95°C; 40 x (30’’-95°C; 30’’-60°C; 20’’-72°C); melting curve 95°C – 60°C – 95°C. A primer list can be found in the supplemental material. Expression levels of target genes were normalized against the housekeeping genes *TIP41-like* and *PP2A* (Czechowski et al., 2005). For every genotype, three biological replicates and two technical duplicates were analysed.

Gene structure and phylogenetic analyses

Complete annotated genomic sequences were obtained from The *Arabidopsis* Information Resource (TAIR – www.arabidopsis.org) for *A. thaliana*, and from the KDRI website (Kazusa DNA Research Institute, Japan; http://www.kazusa.or.jp/lotus/) and the GenBank for *L. japonicus*. BLAST searches were performed on TAIR (http://arabidopsis.org/Blast/index.jsp) with the *L. japonicus* genomic CSG sequences as query. The protein domain organization and the exon-intron structure of the *A. thaliana* homologs of *POLLUX*, *SEC13*, *NUP133* (GenBank accession number: KM269292), *ShRK1* and *ShRK2* are identical to that of their *L. japonicus* counterparts. By sequencing a PCR product amplified from *A. thaliana* wild-type (Col-0) cDNA, we demonstrated that, contrary to the TAIR prediction, this was also the case for *NUP133*. The curated sequence has been submitted to TAIR.

For phylogenetic studies, protein sequences of *A. thaliana* and *L. japonicus* MLD-LRR-RLKs were aligned using MAFFT 7 (Kuraku et al., 2013, Katoh et al., 2017) with default settings. Alignments were used to create phylogenetic trees at the CIPRES web-portal with RAxML 8.2.10 (Stamatakis et al., 2008) for maximum likelihood analyses. For RAxML, the JTT PAM matrix for amino acid substitutions was chosen, and the GTRGAMMA model was used for both bootstrapping and tree inference.

Statistics and data visualisation

All statistical analyses and data plots have been performed and generated with R version 3.0.2 (2013-09-25) "Frisbee Sailing"(Team, 2013) using the packages “Hmisc”(Harrell, 2014) “car”(Fox, 2011), “multcompView”(Graves et al., 2012) and “multcomp”(Hothorn et al., 2008) or Excel. For statistical analysis, data was either subjected to the nonparametric Wilcoxon–Mann–Whitney test with Bonferroni-Holm correction using Col-0 samples as control group, or to the nonparametric Kruskal-Wallis test with Bonferroni correction comparing every group with each other, or was power transformed to improve normality and a one-way ANOVA followed by a Dunnett’s Test with Bonferroni correction was performed using Col-0 samples as control group.

ACKNOWLEDGEMENTS

This work was supported by grants from the German Research Foundation (DFG) and the European Research Commission (ERC) to MP. We thank Birgit Kemmerling for kindly sending us *pskr-1* seeds, Thomas Ott for providing *pAt3g61260:YFP-At3g61260* seeds, Dirk Metzler for help with statistical analyses and Rosa Elena Andrade Aguirre for help with the phylogenetic analyses.

AUTHOR CONTRIBUTION

MKR, ABa, ABi, AAG, CH, RH, TN, MP conceived the research and designed the experiments, ABa, MKR, ABi, FYH, AAG, CH performed the experiments, MKR, ABa, MP wrote the manuscript.

COMPETING FINANCIAL INTERESTS

The authors declare no conflict of interests.

FIGURE SUPPLEMENTS

The submission contains 12 Figure Supplements:

Figure 1 – Figure Supplement 1: Comparison of gene structures and protein domains of *L. japonicus* CSGs and their closest homologs in *A. thaliana.*

Figure 1 – Figure Supplement 2: *A. thaliana* CSGs with encoded proteins and their respective identities / similarities to their *L. japonicus* homologs.

Figure 1 – Figure Supplement 3: Maximum likelihood phylogenetic tree of the extracytoplasmic domains of MLD-LRR-RLKs from *A. thaliana* and *L. japonicus* SYMRK.

Figure 1 – Figure Supplement 4: Maximum likelihood phylogenetic tree of the highly conserved kinase domains of MLD-LRR-RLKs from *A. thaliana* and *L. japonicus* SYMRK.

Figure 1 – Figure Supplement 5: Mutations in *A. thaliana* CSGs reduce the reproductive success of the oomycetal downy mildew pathogen *H. arabidopsidis.*

Figure 1 – Figure Supplement 6: Mutations in *A. thaliana* CSGs do not reduce the number of cells that accommodate haustoria.

Figure 1 – Figure Supplement 7: Mutations in *A. thaliana* CSGs do not impair the reproductive success of the fungal powdery mildew pathogen *E. cruciferarum*.

Figure 2 – Figure Supplement 1: The morphology of *Hpa* haustoria is altered in *A. thaliana* CSG mutants.

Figure 2 – Figure Supplement 2: The morphology of *Hpa* haustoria is only altered in a *A. thaliana* ios1 mutant in the Ler background.

Figure 2 – Figure Supplement 3: The morphology of *Hpa* haustoria is altered in *A. thaliana* CSG mutants.

Figure 2 – Figure Supplement 4: Quantification of haustoria with a fluorescent perihaustorial membrane on *A. thaliana* plants expressing YFP-AtREM1.2.

Figure 3 – Figure Supplement 1: *A. thaliana* CSG mutants do not show developmental or growth defects.

Figure 3 – Figure Supplement 2: Levels of spontaneous or pathogen-induced cell death are unaltered in *A. thaliana* CSG mutants.

SUPPLEMENTAL FILES

The submission contains 3 Supplemental Files:

Supplemental File 1A: Constructs and cloning strategies

Supplemental File 1B: Oligonucleotides

Supplemental Table 1: Mutant lines of *A. thaliana* CSGs and seeds used in the study.

FIGURES

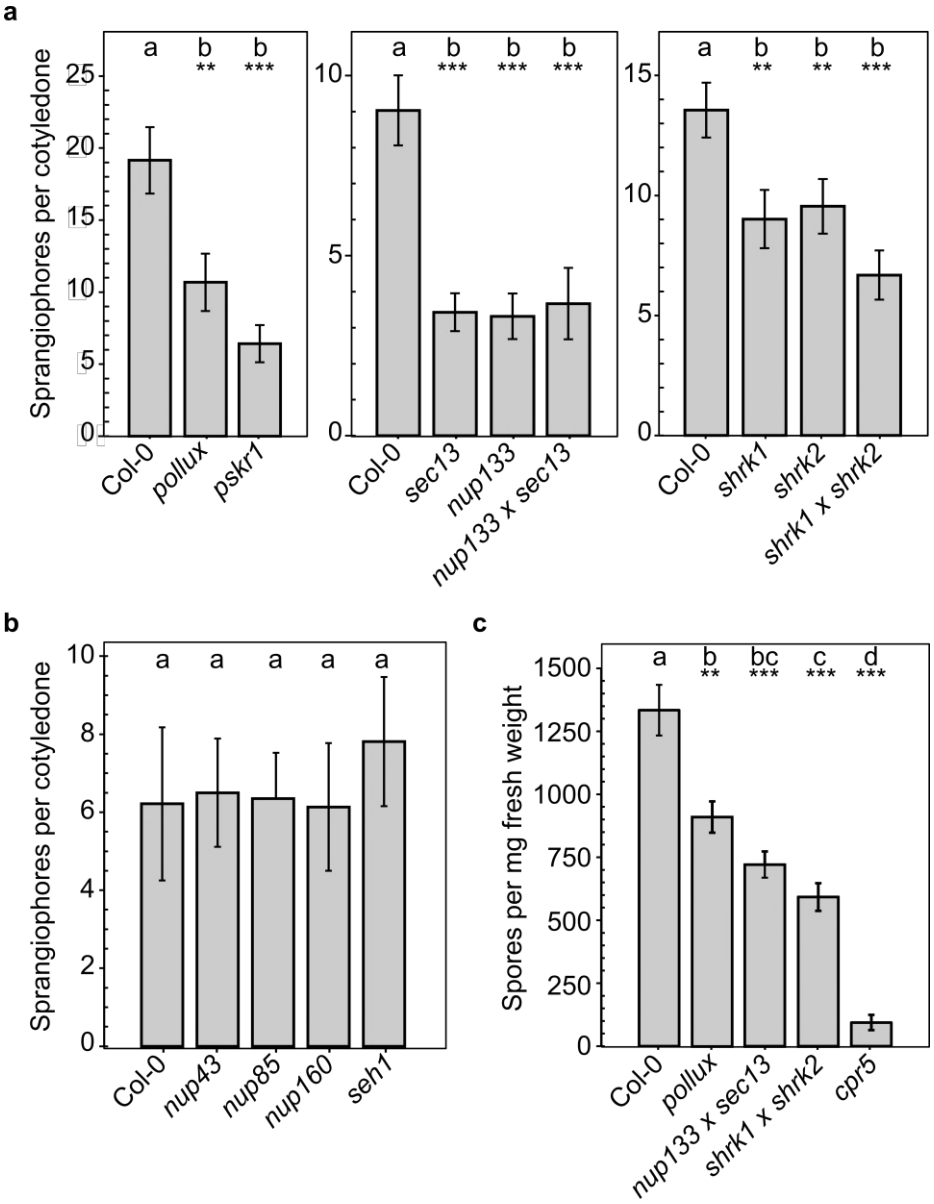

Figure 1: Mutations in *A. thaliana* CSGs reduce the reproductive success of the oomycetal downy mildew pathogen *Hpa*.

(a + b) Bar charts represent the mean number of sporangiophores ± s.e.m on infected cotyledons of *A. thaliana* wild-type (Col-0) or the indicated mutants 4 dpi with *Hpa* isolate NoCo2. **(c)** Bar charts represent the mean number of spores ± s.e.m per mg fresh weight isolated from *A. thaliana* wild-type (Col-0) or the indicated mutants 4 dpi with *Hpa* isolate NoCo2. Stars indicate significant differences to Col-0 (Wilcoxon–Mann–Whitney test with Bonferroni-Holm correction; *, $p < 0.05$; **, $p < 0.01$; ***, $p < 0.001$). Different letters indicate significant differences between groups (Kruskal-Wallis test with Bonferroni correction; $p < 0.05$).

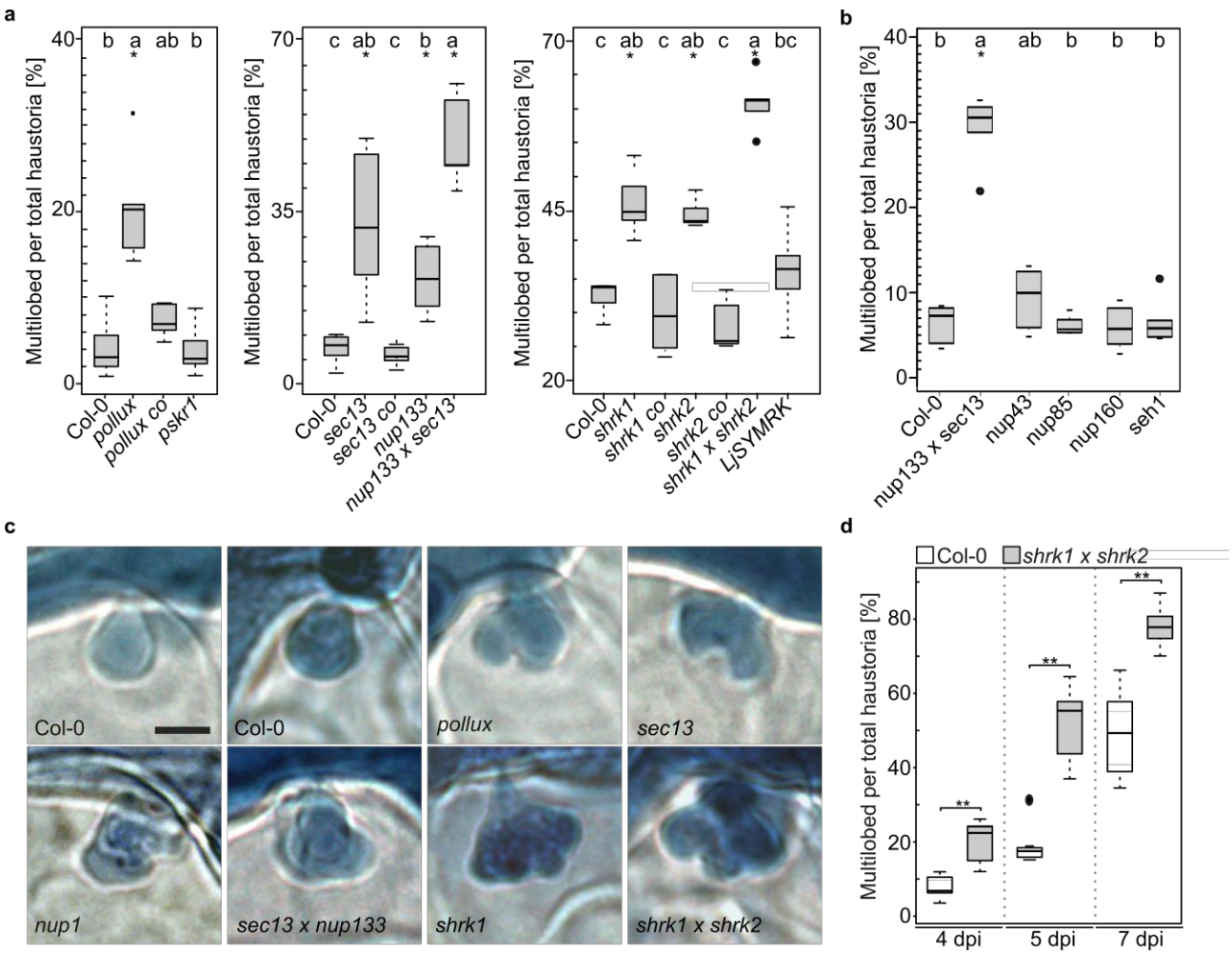

Figure 2: The morphology of *Hpa* haustoria is altered in *A. thaliana* CSG mutants. Boxplots represent the percentage of multilobed haustoria among total haustoria on *A. thaliana* wild-type (Col-0), the indicated mutants and transgenic complementation lines (*pollux co, pPOLLUX:POLLUX; sec13 co, pSEC13:SEC13; shrk1 co, pUbi:ShRK1; shrk2 co, pUbi:ShRK2; LjSYMRK, pUbi:Lotus japonicus SYMRK-mOrange*) 5 dpi with *Hpa* isolate NoCo2 **(a + b)**, or 4, 5 and 7 dpi with *Hpa* isolate NoCo2 **(d)**. **(c)** Representative pictures of intracellular haustoria are displayed. Bars = 25 µm. Black circles, data points outside 1.5 IQR of the upper/lower quartile; bold black line, median; box, IQR; whiskers, lowest/highest data point within 1.5 IQR of the lower/upper quartile. Stars indicate significant differences to Col-0 (Wilcoxon–Mann–Whitney test with Bonferroni-Holm correction; *, $p < 0.05$; **, $p < 0.01$; ***, $p < 0.001$). Different letters indicate significant differences between groups (Kruskal-Wallis test with Bonferroni correction; $p < 0.05$).

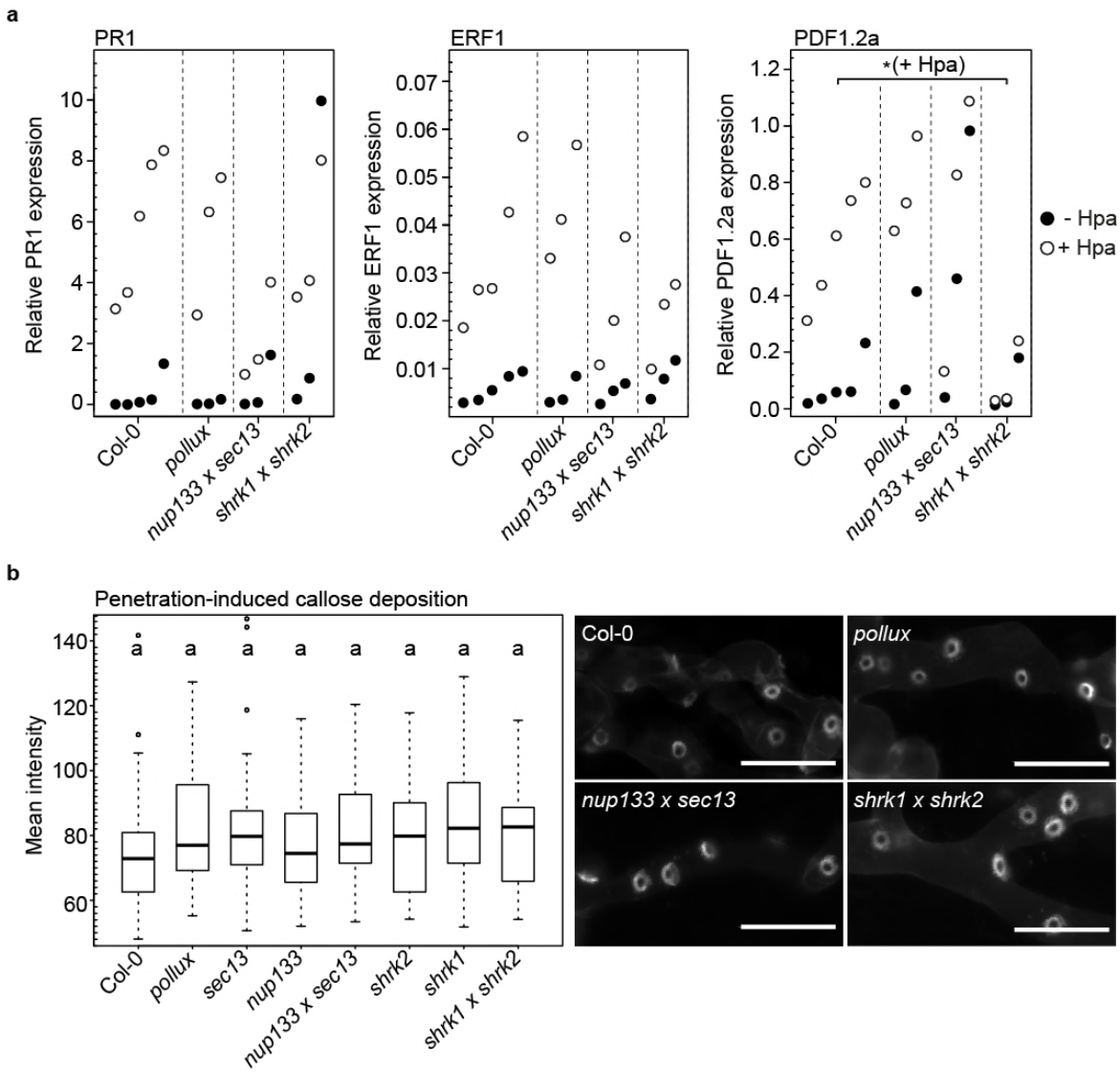

Figure 3: Activation of defence responses in response to *Hpa* infection is unaltered in *A. thaliana* CSG mutants.

(a) Expression of *PR1*, *ERF1* or *PDF1.2a* relative to the housekeeping genes *TIP41-like* and *PP2A* in mock-treated samples (black circles) or in *Hpa*-infected samples (empty circles) was determined in three biological replicates for each genotype by qPCR. Stars indicate significant differences to Col-0 (Dunnett's Test with Bonferroni correction; *, $p < 0.05$). **(b)** Bar charts represent the mean intensity of callose deposition in leaves of *A. thaliana* wild-type (Col-0) or the indicated mutants 4 dpi with *Hpa* isolate NoCo2. Circles, data points outside 1.5 IQR of the upper/lower quartile; bold black line, median; box, IQR; whiskers, lowest/highest data point within 1.5 IQR of the lower/upper quartile. No significant differences between Col-0 and the mutants or between any of the groups could be observed with a Wilcoxon–Mann–Whitney test with Bonferroni-Holm correction or a Kruskal-Wallis test with Bonferroni correction. Representative pictures of haustoria-associated callose deposition at the neck band of *Hpa* haustoria growing on the indicated mutants are shown on the right. Bars, 25 µm.

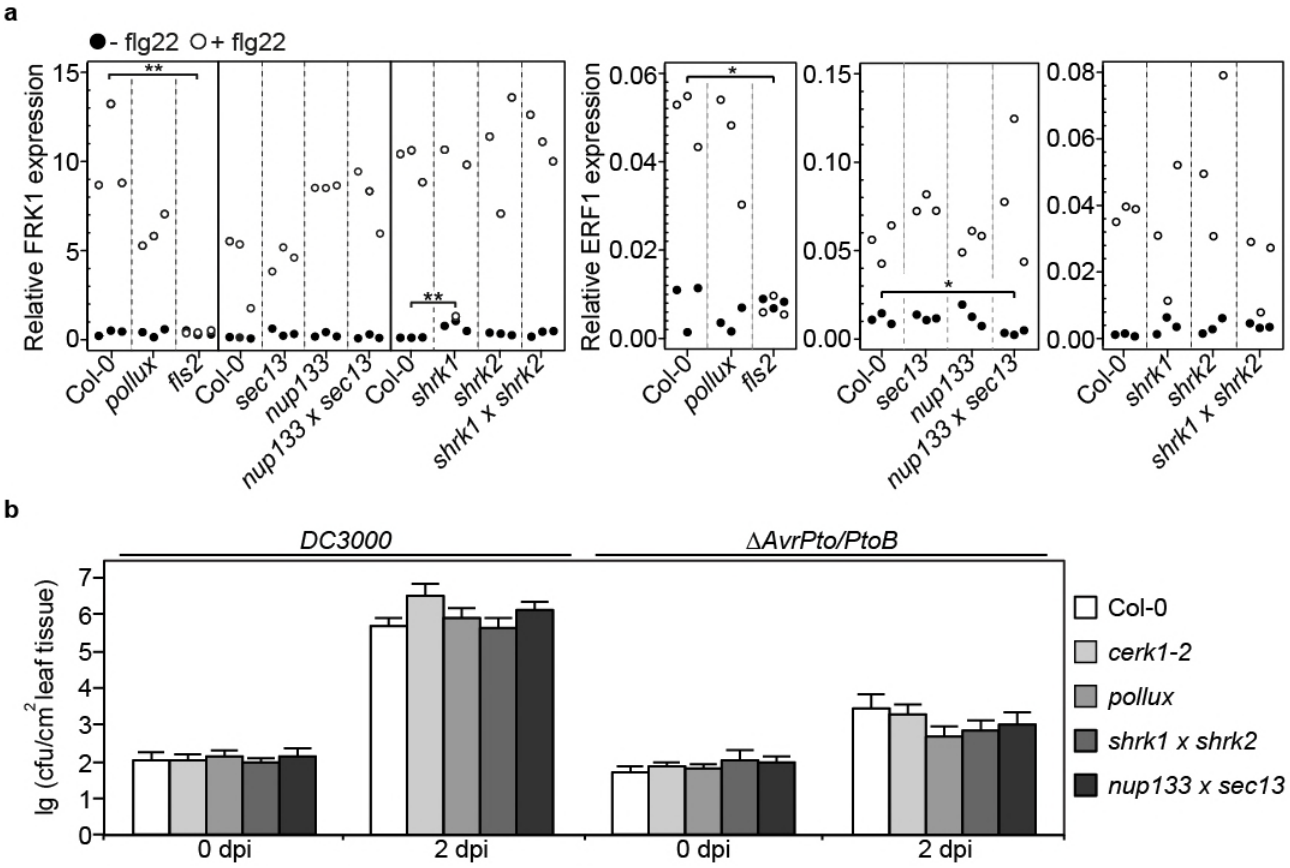

Figure 4: Expression of flg22-inducible genes as well as growth of the bacterial pathogen *Pseudomonas syringae* are not affected in *A. thaliana* CSG mutants.

(a) Expression of *FRK1* and *ERF1* relative to the housekeeping genes *TIP41-like* and *PP2A* in mock-treated samples (black circles) or in flg22-treated samples (empty circles) was determined in three biological replicates for each genotype by qPCR. The *fls2* mutant served as negative control. Stars indicate significant differences to Col-0 (Dunnett's Test with Bonferroni correction; *, $p < 0.01$; **, $p < 0.001$). **(b)** Bacterial density of *Pto* DC3000 or *Pto* DC3000 Δ*AvrPto/PtoB* on *A. thaliana* wild-type (Col-0) or the indicated mutants was determined as colony forming units per cm^2 2 dpi. Data represent means ± s.d. of six replicate measurements/genotype/data point. Results from one representative of at least four independent experiments are shown.

FIGURE SUPPLEMENTS

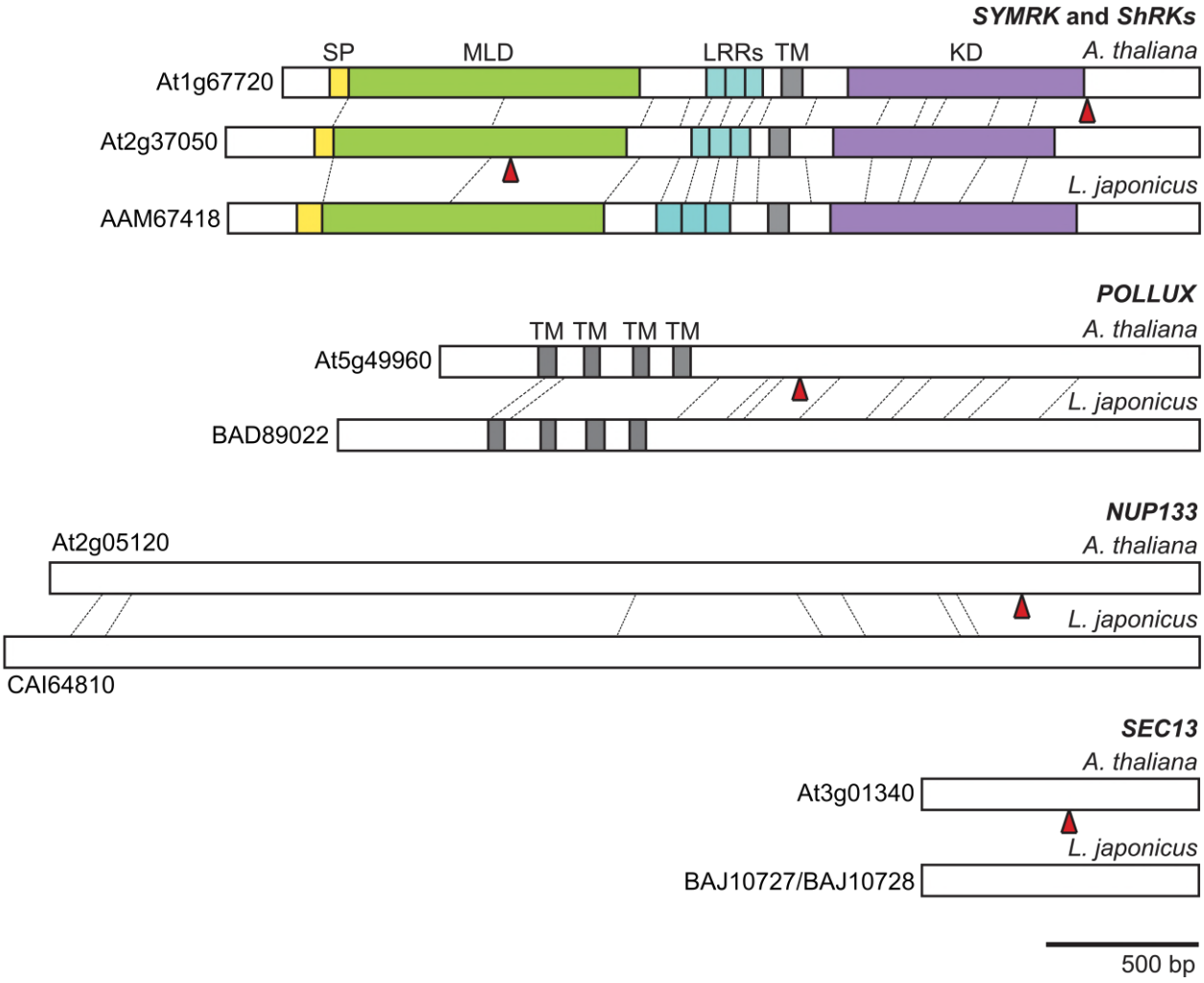

Figure 1 – Figure Supplement 1: Comparison of gene structures and protein domains of *L. japonicus* CSGs and their closest homologs in *A. thaliana.*

TAIR/GenBank protein identifiers are shown; dashed lines, positions of introns in the original gene sequence; red triangles, positions of T-DNA insertion in the respective mutants; SP, signal peptide; MLD, malectin-like domain; LRRs, leucine-rich repeats; TM, transmembrane domain; KD, kinase domain.

Gene	*L. japonicus* homolog (NCBI mRNA/protein IDs)	Gene ID	NASC ID	Protein Identity / Similarity To *L. japonicus*
POLLUX	AB162158 / BAD89022	At5g49960	N566135	71 / 82
SEC13	AB506697 / BAJ10727 - AB506698 / BAJ10728	At3g01340	N662322	80-82 / 92-91
NUP133	AJ890251 / CAI64810	At2g05120	N565761	55 / 71
SEH1	AB506696 / BAJ10726	At1g64350	N653094	64 / 78
NUP43	n.d.	At4g30840	N803490	n.d.
NUP85	AB284835 / BAF45348	At4g32910	N613274	61 / 75
NUP160	n.d.	At1g33410	N624418	n.d.
ShRK1	(*SYMRK*) AF492655 / AAM67418	At1g67720	N467036	33 (48KD) / 49 (68KD)
ShRK2		At2g37050	N643700	34 (48KD) / 50 (68KD)

Figure 1 – Figure Supplement 2: *A. thaliana* CSGs with encoded proteins and their respective identities / similarities to their *L. japonicus* homologs.

Sequence identifiers and identities / similarities shared between the protein sequences of *A. thaliana* CSGs and those of their respective *L. japonicus* counterparts. The numbers for AtSEC13 indicate the identity / similarity of its amino acid sequence to each of the two predicted LjSEC13 proteins. For ShRK1 and ShRK2, numbers in brackets refer to their kinase domain (KD) only. n.d., not detected. NASC ID: insertion mutant identifier.

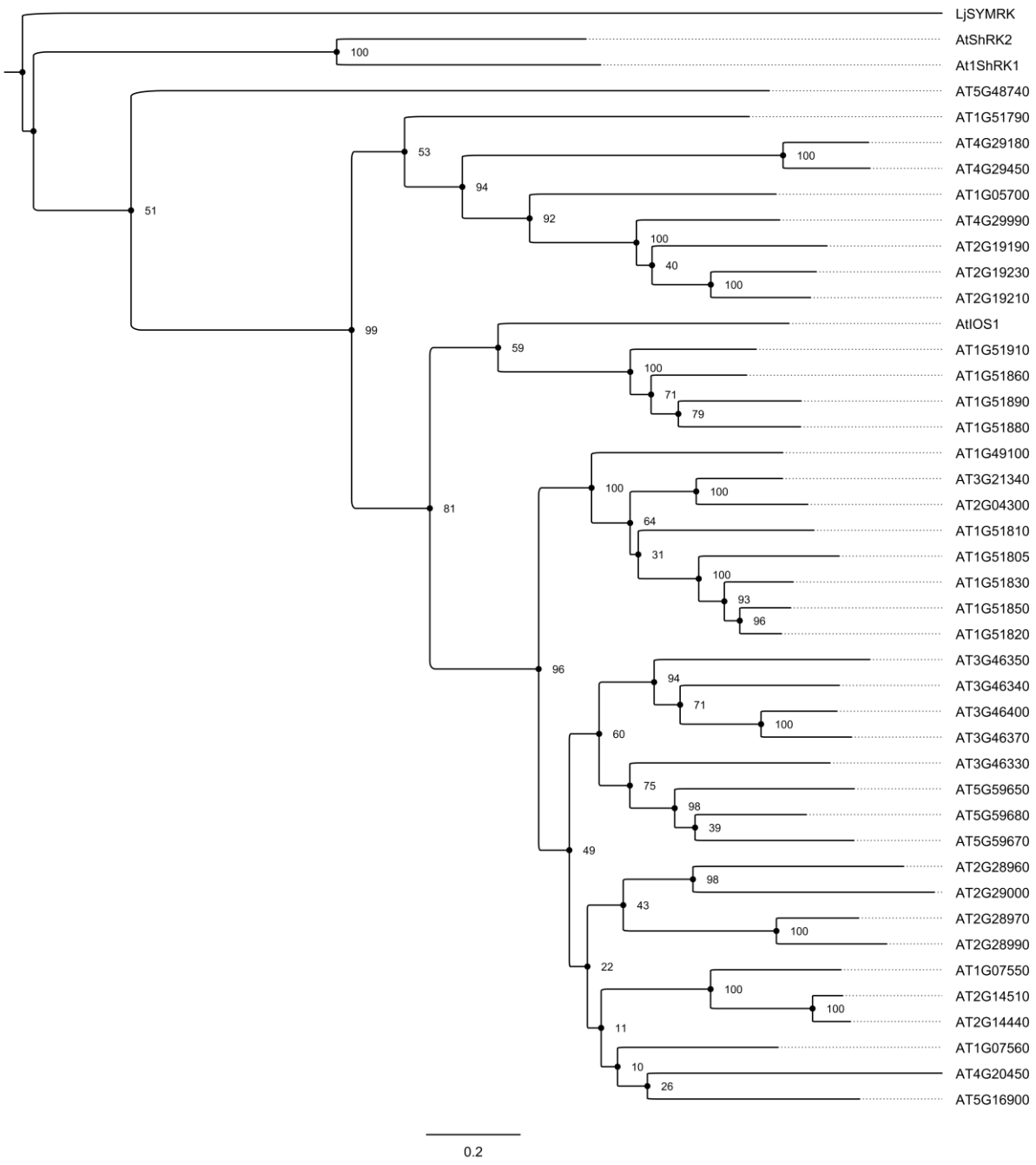

Figure 1 – Figure Supplement 3: Maximum likelihood phylogenetic tree of the extracytoplasmic domains of MLD-LRR-RLKs from *A. thaliana* and *L. japonicus* SYMRK.

The specific domain composition featuring a MLD followed by the conserved gly-asp-pro-cys (GDPC) motif known to be required for the proper establishment of the symbiotic program in the root epidermis (Kosuta et al., 2011, Antolin-Llovera et al., 2014), and LRRs is not restricted to SYMRK but can also be found in 42 of the 50 members of LRR I-RLKs present in *A. thaliana*, where this family underwent a recent expansion (Shiu and Bleecker, 2003, Hok et al., 2011). A maximum likelihood phylogenetic tree based on the extracytoplasmic regions (excluding the signal peptides) of 42 MLD-LRR-RLK proteins from *A. thaliana* and SYMRK from *L. japonicus*. Numbers on each node represent the respective bootstrap values. Bar, relative genetic distance (arbitrary unit).

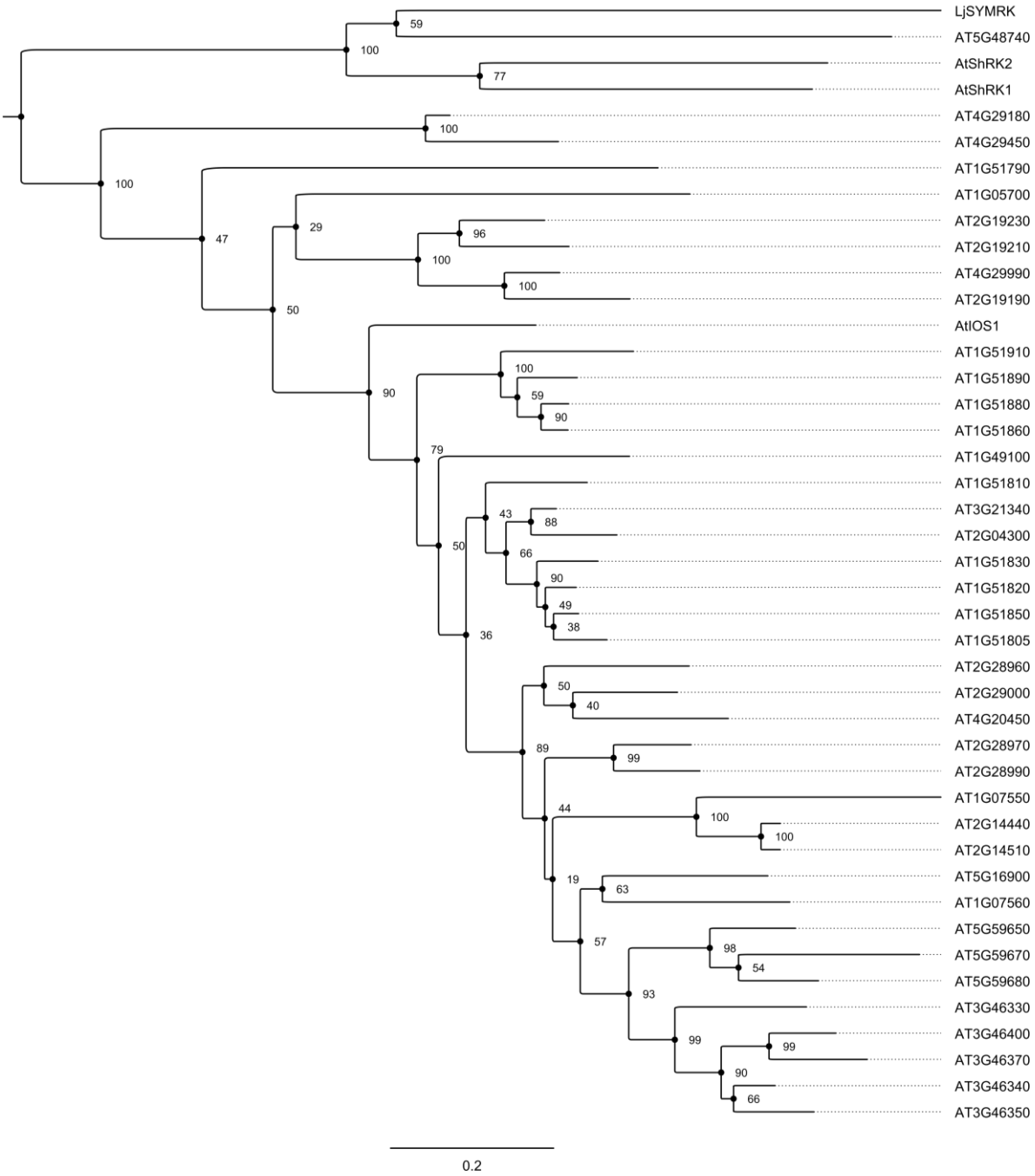

Figure 1 – Figure Supplement 4: Maximum likelihood phylogenetic tree of the highly conserved kinase domains of MLD-LRR-RLKs from *A. thaliana* and *L. japonicus* SYMRK.

A maximum likelihood phylogenetic tree based on the highly conserved kinase domains of 42 MLD-LRR-RLK proteins from *A. thaliana* and SYMRK from *L. japonicus*. Numbers on each node represent the respective bootstrap values. Bar, relative genetic distance (arbitrary unit).

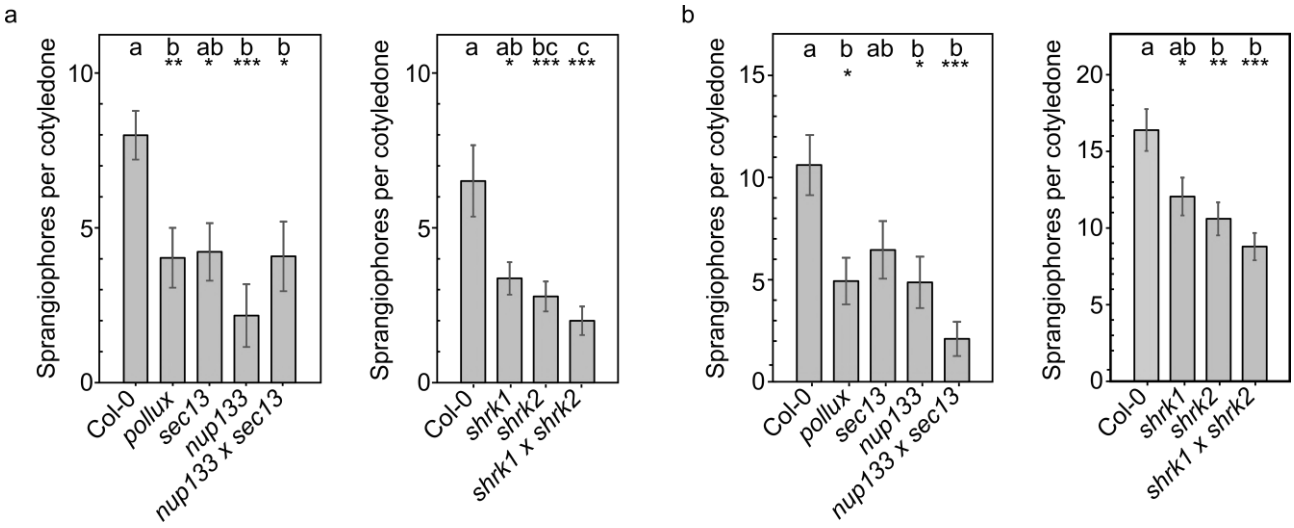

Figure 1 – Figure Supplement 5: Mutations in *A. thaliana* CSGs reduce the reproductive success of the oomycetal downy mildew pathogen *H. arabidopsidis.*

Bar charts represent the mean number of sporangiophores ± s.e.m on infected cotyledons of *A. thaliana* wild-type (Col-0) or the indicated mutants 4 dpi with *Hpa* isolate NoCo2 in two additional replicates **(a + b)**. Stars indicate significant differences to Col-0 (Wilcoxon–Mann–Whitney test with Bonferroni-Holm correction; *, $p < 0.05$; **, $p < 0.01$; ***, $p < 0.001$). Different letters indicate significant differences between groups (Kruskal-Wallis test with Bonferroni correction).

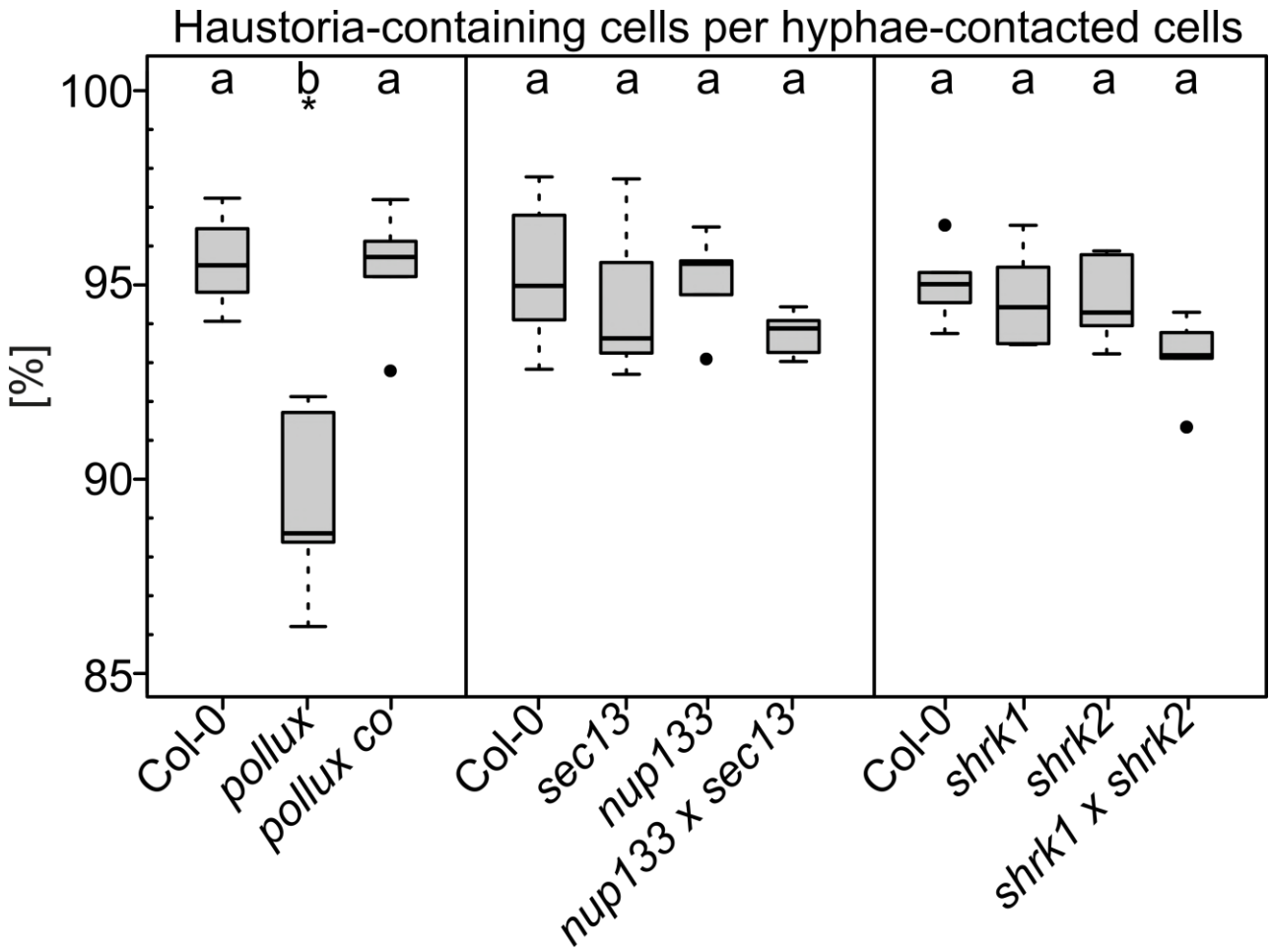

Figure 1 – Figure Supplement 6: Mutations in *A. thaliana* CSGs do not reduce the number of cells that accommodate haustoria.

Boxplots represent the percentage of haustoria-containing cells per cells contacted by hyphae on leaves of *A. thaliana* wild-type (Col-0), the indicated mutants and the transgenic complementation lines (*pollux co*, *pPOLLUX:POLLUX*) 5 dpi with *Hpa* isolate NoCo2. Black circles, data points outside 1.5 IQR of the upper/lower quartile; bold black line, median; box, IQR; whiskers, lowest/highest data point within 1.5 IQR of the lower/upper quartile. Stars indicate significant differences to Col-0 (Wilcoxon–Mann–Whitney test with Bonferroni-Holm correction; *, $p < 0.05$; **, $p < 0.01$; ***, $p < 0.001$). Different letters indicate significant differences between groups (Kruskal-Wallis test with Bonferroni correction)

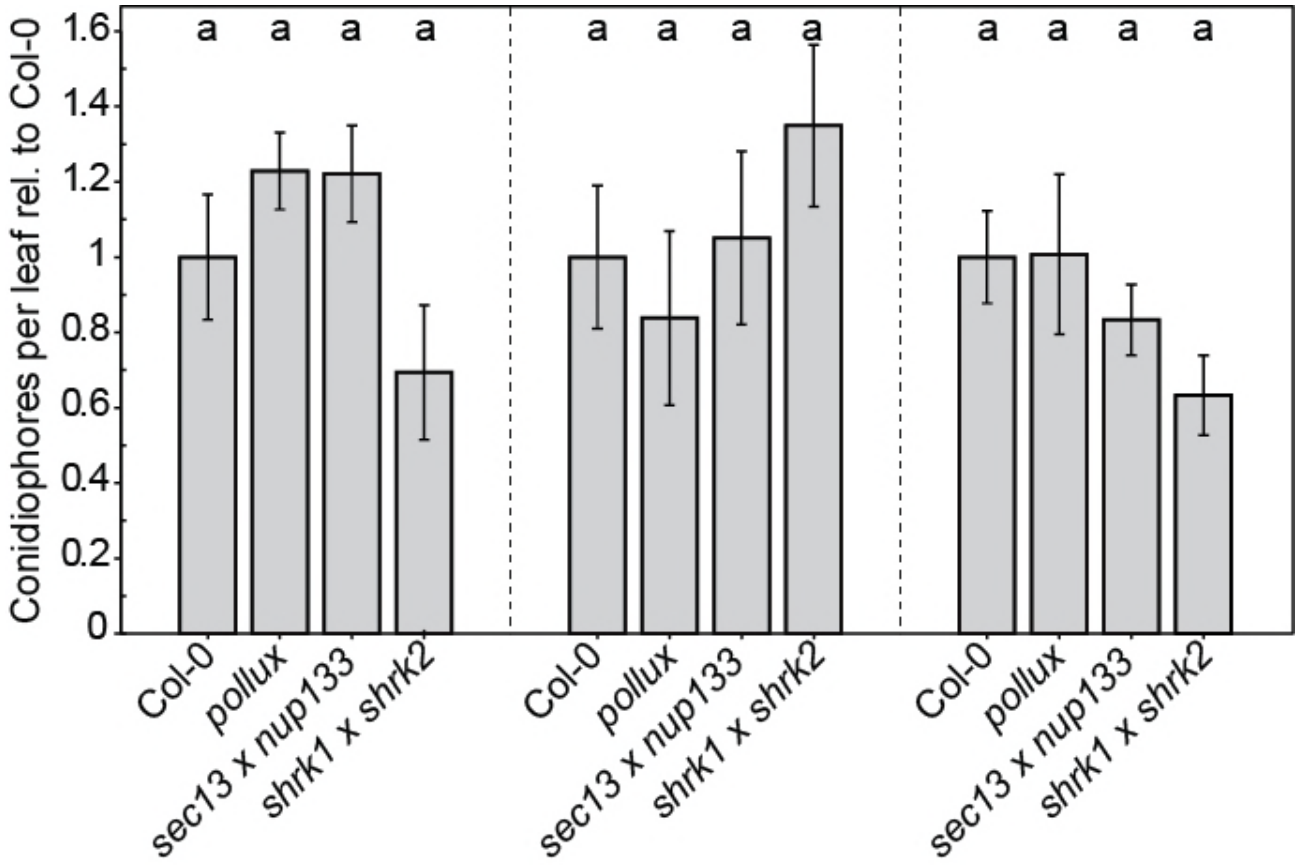

Figure 1 – Figure Supplement 7: Mutations in *A. thaliana* CSGs do not impair the reproductive success of the fungal powdery mildew pathogen *E. cruciferarum*.

Bar charts represent the mean number of conidiophores ± s.e.m on leaves of the indicated mutants relative to the wild-type (Col-0) 5 dpi with *E. cruciferarum* for three independent replicates. No significant differences to Col-0 were detected (Wilcoxon–Mann–Whitney test with Bonferroni-Holm correction; *, $p < 0.05$; **, $p < 0.01$; ***, $p < 0.001$). No significant differences between groups were detected (Kruskal-Wallis test with Bonferroni correction; $p < 0.05$).

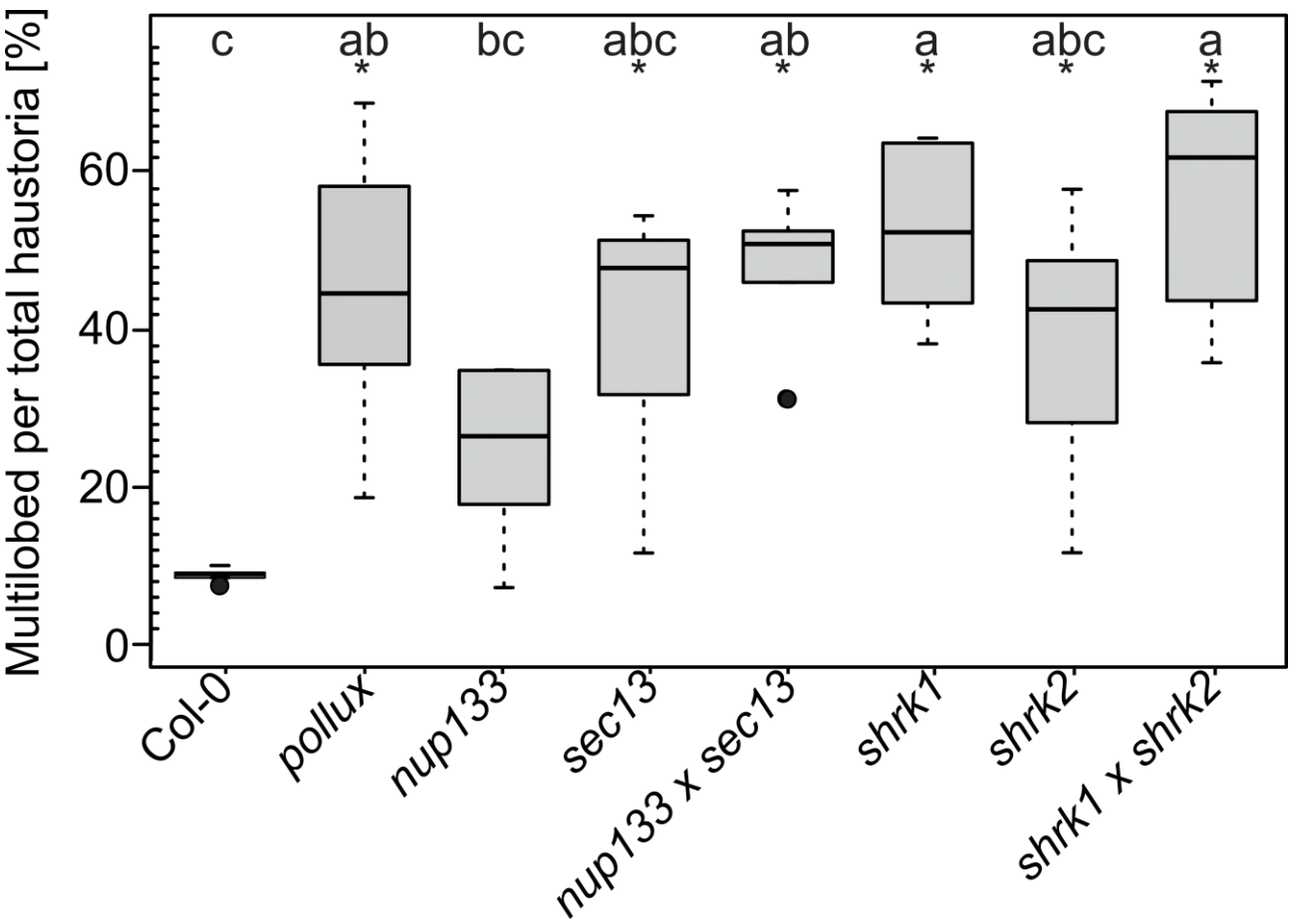

Figure 2 – Figure Supplement 1: The morphology of *Hpa* haustoria is altered in *A. thaliana* CSG mutants.

Boxplots represent the percentage of multilobed haustoria among total haustoria on *A. thaliana* wild-type (Col-0) or the indicated mutants 5 dpi with *Hpa* isolate NoCo2. Black circles, data points outside 1.5 IQR of the upper/lower quartile; bold black line, median; box, IQR; whiskers, lowest/highest data point within 1.5 IQR of the lower/upper quartile. Stars indicate significant differences to Col-0 (Wilcoxon–Mann–Whitney test with Bonferroni-Holm correction; *, $p < 0.05$; **, $p < 0.01$; ***, $p < 0.001$). Different letters indicate significant differences between groups (Kruskal-Wallis test with Bonferroni correction).

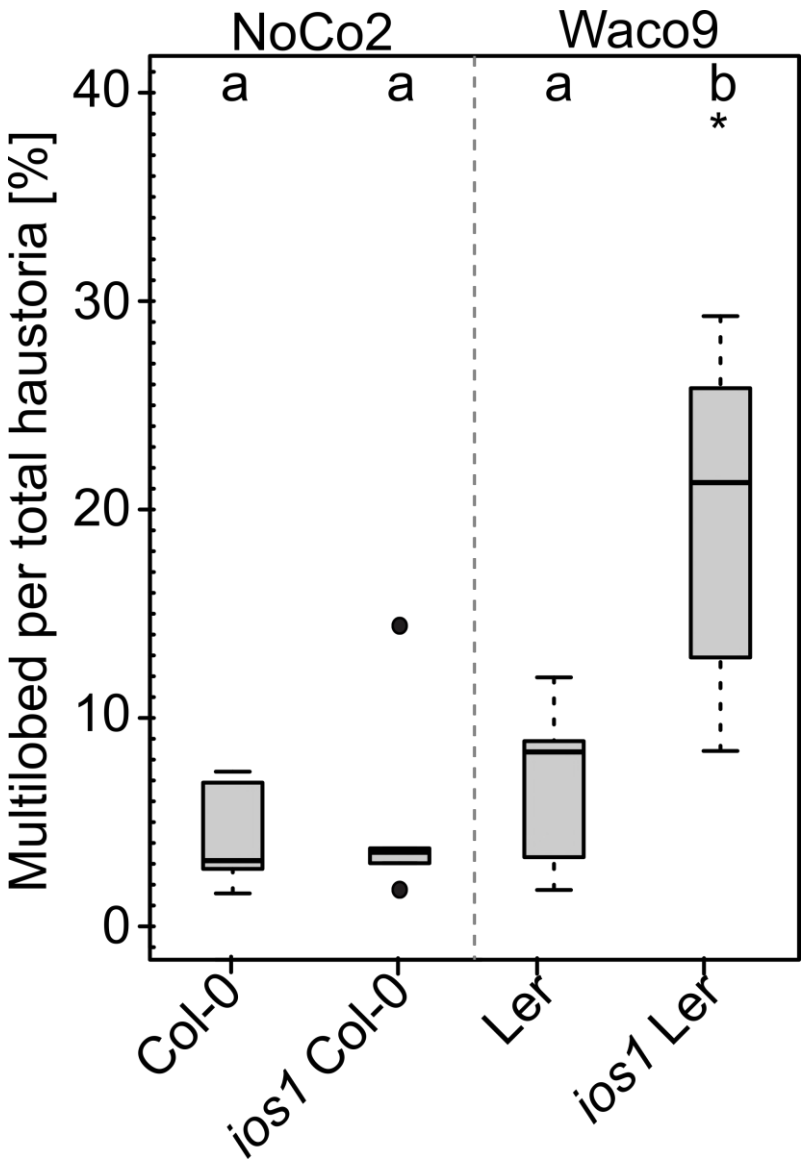

Figure 2 – Figure Supplement 2: The morphology of *Hpa* haustoria is only altered in a *A. thaliana ios1* mutant in the Ler background.

Boxplots represent the percentage of multilobed haustoria among total haustoria on *A. thaliana* wild-type (Col-0; Ler), and *ios1* mutant lines 5 dpi with *Hpa* isolate NoCo2 (a), 5 dpi with *Hpa* isolate NoCo2 and Waco9. Black circles, data points outside 1.5 IQR of the upper/lower quartile; bold black line, median; box, IQR; whiskers, lowest/highest data point within 1.5 IQR of the lower/upper quartile. Stars indicate significant differences to Col-0 (Wilcoxon–Mann–Whitney test with Bonferroni-Holm correction; *, $p < 0.05$; **, $p < 0.01$; ***, $p < 0.001$). Different letters indicate significant differences between groups (Kruskal-Wallis test with Bonferroni correction; $p < 0.05$).

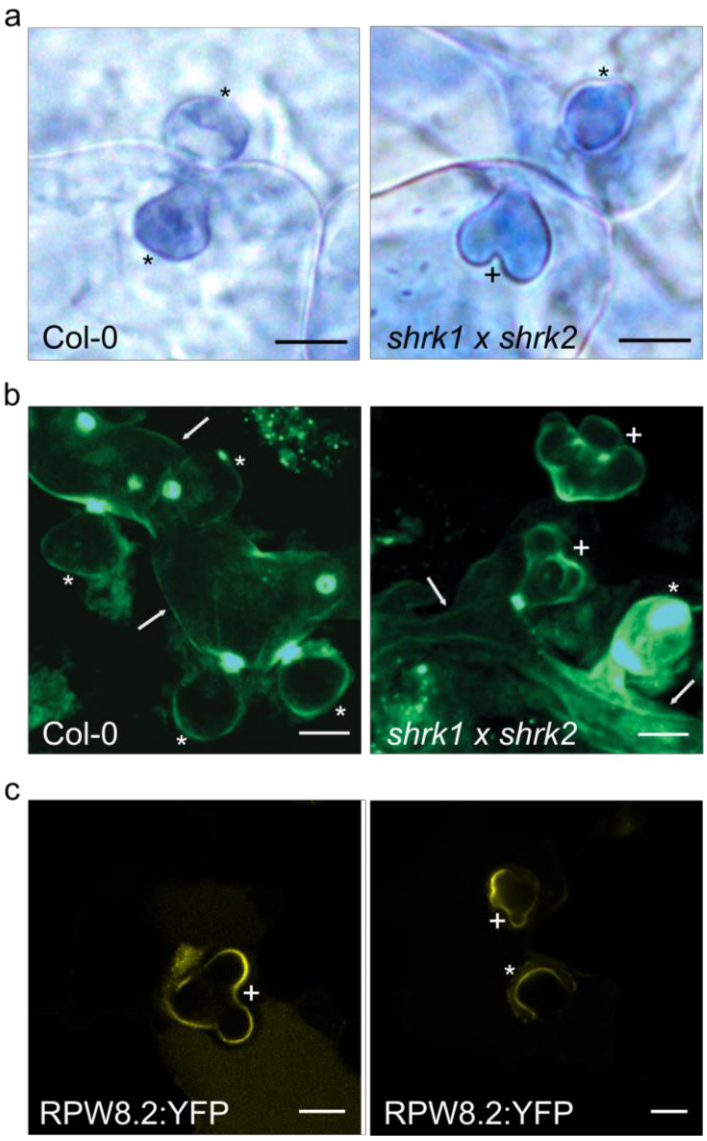

Figure 2 – Figure Supplement 3: The morphology of *Hpa* haustoria is altered in *A. thaliana* CSG mutants.

(a) Light microscopy of Technovit section of *A. thaliana* wild-type (Col-0) or the *shrk1 x shrk2* double mutant 7 dpi with *Hpa* isolate NoCo2. Bars, 10 µm. **(b)** Confocal light scanning microscopy of leaves of *A. thaliana* wild-type (Col-0) or the *shrk1 x shrk2* double mutant stained with aniline-blue 5 dpi with *Hpa* isolate NoCo2. For every haustorium, the entry point can be identified by the formation of the usually bright callose neck. Bars, 25 µm. **(c)** Confocal light scanning microscopy of leaves of *A. thaliana* wild-type (Col-0) expressing RPW8.2:YFP, which localises to the perihaustorial membrane. *, round haustoria; +, multilobed haustoria; arrows, hyphae. Bars, 10 µm.

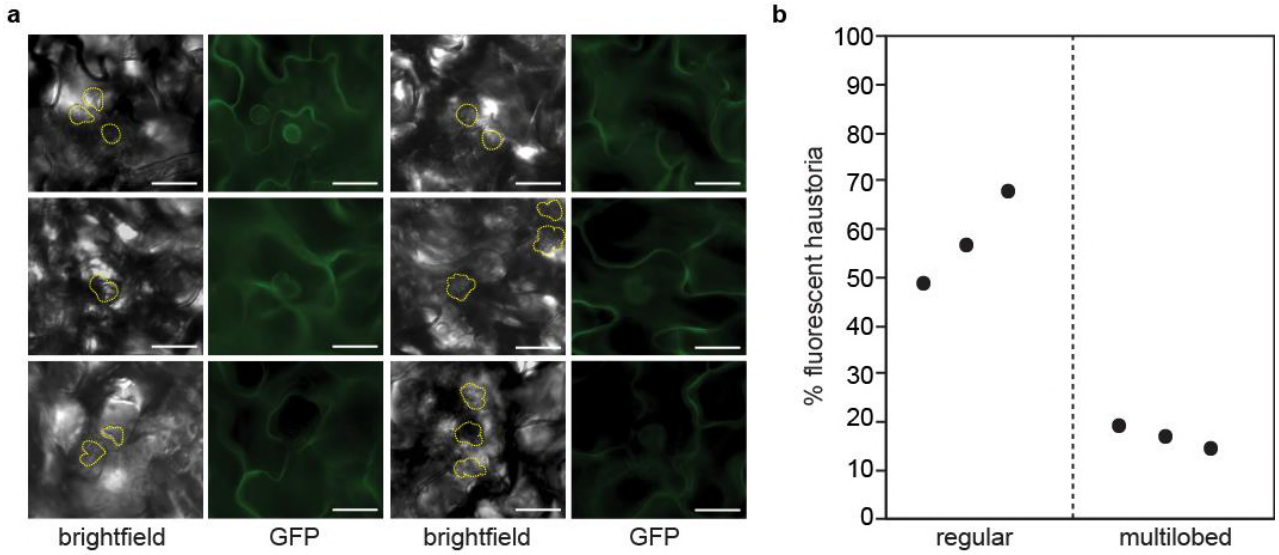

Figure 2 – Figure Supplement 4: Quantification of haustoria with a fluorescent perihaustorial membrane on *A. thaliana* plants expressing YFP-AtREM1.2.

(a) *A. thaliana* plants expressing N-terminally YFP-tagged AtREM1.2 under the control of its native promoter were inspected with an epifluorescence microscope 8 dpi with *Hpa* isolate NoCo2. Representative pictures of YFP-positive and YFP-negative (completely dark) haustoria are shown. Yellow dashed lines delimitate haustoria in the bright field images. Bars, 25 µM. **(b)** Graph represents the percentage of fluorescent haustoria as a function of morphology (1st replicate, 49 % of single-lobed haustoria show fluorescence/19 % of multilobed haustoria show fluorescence; 2nd replicate, 56 % single-lobed/17 % multilobed, 3rd replicate: 68 % single-lobed/14 % multilobed).

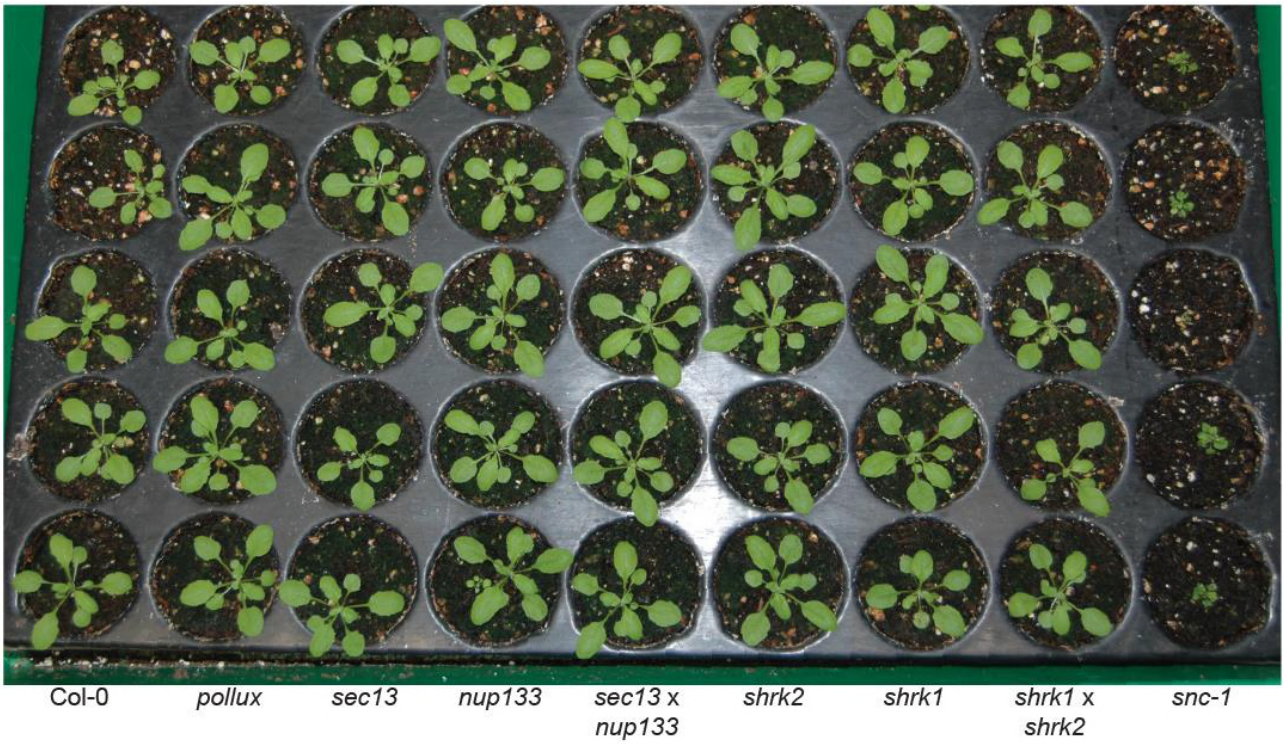

Figure 3 – Figure Supplement 1: *A. thaliana* CSG mutants do not show developmental or growth defects.

3-week-old *A. thaliana* wild-type (Col-0) plants grown alongside the indicated mutant lines under long day conditions. The dwarf phenotype of *snc1* is included on the far right for comparison.

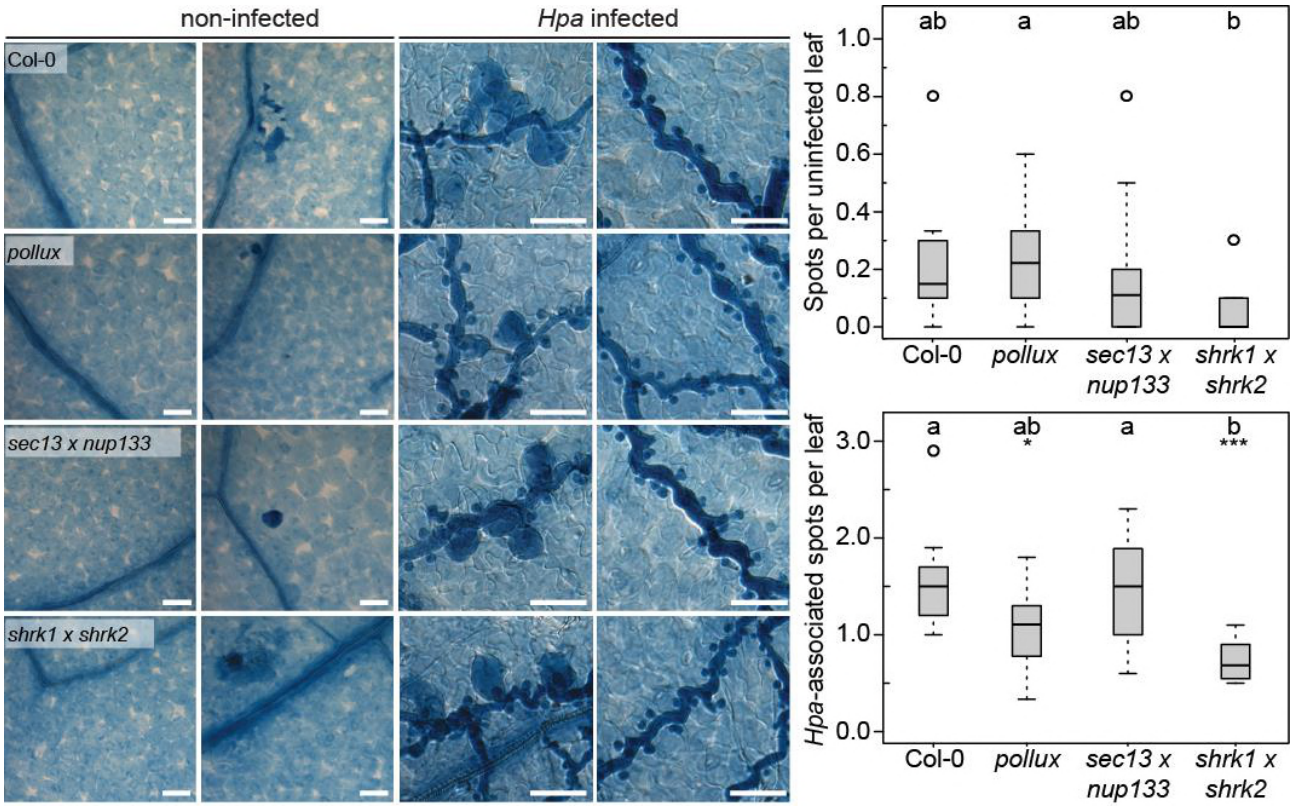

Figure 3 – Figure Supplement 2: Levels of spontaneous or pathogen-induced cell death are unaltered in *A. thaliana* CSG mutants.

Differential interference contrast microscopy of *A. thaliana* wild-type (Col-0) and CSG mutant leaves stained with trypan-blue lactophenol 4 dpi with *Hpa* isolate NoCo2. First column, non-infected without cell death; second column, non-infected with random cell death; third column, infected with cell death in, or adjacent to, haustoria-containing cells; fourth column, infected without cell death. Bars, 25 µm**.** Boxplots represent the number of random (upper graph) or *Hpa*-associated (lower graph) cell death spots per leaf on *A. thaliana* wild-type (Col-0) or the indicated mutants 5 dpi with *Hpa* isolate NoCo2. Circles, data points outside 1.5 IQR of the upper/lower quartile; bold black line, median; box, IQR; whiskers, lowest/highest data point within 1.5 IQR of the lower/upper quartile. Stars indicate significant differences to Col-0 (Wilcoxon–Mann–Whitney test with Bonferroni-Holm correction; *, $p < 0.05$; **, $p < 0.01$; ***, $p < 0.001$). Different letters indicate significant differences between groups (Kruskal-Wallis test with Bonferroni correction; $p < 0.05$).

SUPPLEMENTAL INFORMATION

Supplemental File 1A: Constructs and cloning strategy.

Constructs labelled with "GG" were generated via Golden Gate cloning. For details on assembly method, general modules and plasmids (G*xx*, BB*xx*), see (Binder et al., 2014). Golden Gate constructs contain silent mutations to facilitate cloning.

Entry clones / Golden Gate Level I & Level II plasmids (LI & LII)

Name	Description
pENTR-pSEC13:SEC13	Phusion PCR product consisting of *SEC13* genomic construct amplified from *A. thaliana* gDNA with sec13co_FW and sec13co_RV, cloned into pENTR/D-TOPO (Invitrogen) via TOPO reaction.
LI A-C *pPOLLUX* (GG)	LI promoter element of *POLLUX* (1523 bp). Assembled from 2 PCR fragments amplified from *A. thaliana* gDNA by BpiI cut ligation into LI-BpiI vector. Fragment 1: AtPol-Pro1+ & AtPol-Pro2- Fragment 2: AtPol-Pro3+ & AtPol-Pro4-
LI C-D *POLLUX* (GG)	LI element containing genomic *POLLUX*. Assembled from 2 PCR fragments amplified from *A. thaliana* gDNA by BpiI cut ligation into LI-BpiI vector. Fragment 1: AtPol1+ & AtPol2- Fragment 2: AtPol3+ & AtPol4-
LII F 1-2 *pPOLLUX:POLLUX* (GG)	Assembled by BsaI cut ligation from: LI A-C pPOLLUX + LI C-D POLLUX + LI dy D-E (BB8) + LI E-F 35S-T (G59) + LI F-G neo (G3) + LIIc F1-2 (BB30)
LII R 3-4 *p35S:mCherry* (GG)	Assembled by BsaI cut ligation from: LI A-B p35S (G5) + LI dy B-C (BB6) + LI C-D mCherry (G23) + LI dy D-E (BB8) + LI E-F nos-T (G6) + LI dy F-G (G9) + LIIc R 3-4 (BB33)
LII R 5-6 *p35S:mCherry* (GG)	Assembled by BsaI cut ligation from: LI A-B p35S (G5) + LI dy B-C (BB6) + LI C-D mCherry (G23) + LI dy D-E (BB8) + LI E-F HSP-T(G45) + LI dy F-G (G9) + LIIc R 5-6 (BB37)

LI A-C *ShRK1* (GG)	Full length genomic DNA from ATG to codon prior to STOP (bases 1-4360); silent mutations introduced to remove type IIS restriction sites; obtained by gene synthesis (GenScript)
LI A-C *ShRK2* (GG)	Full length genomic DNA from ATG to codon prior to STOP (bases 1-4185); silent mutations introduced to remove type IIS restriction sites; obtained by gene synthesis (GenScript)
LII F 1-2 *pUBi: ShRK1-YFP* (GG)	Assembled by BsaI cut ligation from: LI A-B pUBi (G7) + LI dy B-C (G4) + LI A-C ShRK1 + LI D-E YFP (G12) + LI E-F 35S-T (G59) + LI F-G hygro (G94) + LIIc F 1-2 (BB30)
LII F 1-2 *pUBi: ShRK2-YFP* (GG)	Assembled by BsaI cut ligation from: LI A-B pUBi (G7) + LI dy B-C (G4) + LI A-C ShRK2 + LI D-E YFP (G12) + LI E-F 35S-T (G59) + LI F-G hygro (G94) + LIIc F 1-2 (BB30)

Plasmids for stable transformation of *A. thaliana*

Name	**Description**
pSEC13:SEC13 + free mCherry	LR reaction of *pENTR-pSEC13:SEC13* and PMDC99 (Curtis and Grossniklaus, 2003); hygromycin resistance
pPOLLUX:POLLUX + free mCherry (GG)	Assembled by BpiI cut ligation from: LII F 1-2 pPOLLUX:POLLUX + LII 2-3 ins (BB43) + LII R 3-4 p35S:mCherry + LII dy 4-6 (BB41) + LIIIα fin (BB45); kanamycin resistance
pUBi:ShRK1-YFP + free mCherry (GG)	Assembled by BpiI cut ligation from: LII F 1-2 pUBi:ShRK1 + LII 2-3 ins (BB43) + LII R 3-4 p35S-mCherry + LII dy 4-6 (BB41) + LIIIα fin (BB45); hygromycin resistance
pUBi:ShRK2-YFP + free mCherry (GG)	Assembled by BpiI cut ligation from: LII F 1-2 pUBi:ShRK2 + LII 2-3 ins (BB43) + LII R 3-4 p35S-mCherry + LII dy 4-6 (BB41) + LIIIα fin (BB45); hygromycin resistance
pUbi:SYMRK-mOrange (GG)	Antolin-Llovera et al., 2014

657 **Supplemental File 1B: Oligonucleotides**

Expression analysis

Target	Reference
PP2A	(Czechowski et al., 2005)
TIP41-like	(Czechowski et al., 2005)
FRK1	(Asai et al., 2002)
PDF1.2a	(Moffat et al., 2012)
ERF1	(Solano et al., 1998)
PR1	(Onate-Sanchez et al., 2007)

Plasmid construction

Name	Primer sequence (5’ - 3’)
sec13co_FW	CACCGGGAACACGGGAGAATAG
sec13co_RV	TTTTGCAATCTCTGTTGTCTGA
N133-pro2_FW	AGGGTCTCACACCGTTTTGAAAGACGGCATATTATGG
N133-pro3_RV	AGGGTCTCATACAAGGTCTTTTATTGCTTAAAACTCT
N133-pro3_FW	AGGGTCTCATGTACATTTATTTGTTTTCATTGATTG
N133_Pro4_RV	AGGGTCTCAACATTTTAAACCAGGAAGAGAGCGA
N133_ATG_FW	AGGGTCTCAATGTTCTCTCCATTGACGAAGA
N133_mut_1b_RW	AGGGTCTCATTTCTTTATCCATTCCACCGGA
N133_mut_1_FW	GGGGTCTCAGAAACCTGTCTTTCTTGGTTTATT
N133_mut_2_RW	GGGGTCTCAGCGACCGAGAAGCCCT
N133_mut_2_FW	GGGGTCTCATCGCGTAGTCCTGTTGGTGT
N133_e3_RV	AGGGTCTCACTCTCTGCAGTTGAGTTCCTAGTG
N133_e3_FW	AGGGTCTCAAGAGCCTGCGAACTCTCAAA
N133_3'UTR2_RV	AGGGTCTCACCTTGGTAGATTCGATACATCATAAAGAGG
AtPol-Pro1+	ATGAAGACTTTACGGGTCTCAGCGGAGCCCAATGACTTCCCACAC
AtPol-Pro2-	TAGAAGACAAATGACTACAGTTTCATGCCACCA
AtPol-Pro3+	ATGAAGACTTTCATCATTATGCTCATCTTGAATATGT
AtPol-Pro4-	TAGAAGACAACAGAGGTCTCAGGTGCGGGTTGAAGTAAGTAAATTGAGA

AtPol1+	ATGAAGACTTTACGGGTCTCACACCATGCCGATTCATACCCCTAGA
AtPol2-	TAGAAGACAACATCTTCTTTCTTCTGATTTGTTCGT
AtPol3+	ATGAAGACTTGATGTTCCTTTGAAGAAGAGACTAGC
AtPol4-	ATGAAGACTTCAGAGGTCTCACCTTCTGACTTGAGGCGATGACAAC

Supplemental Table 1: Mutant lines of *A. thaliana* CSGs and seeds used in the study.

Gene and ID	Mutant line	Seedbag
ShRk1 (At1g67720)	GK-699C04 2	1898
ShRk2 (At2g37050)	SALK_143700	1902
ShRk1 (At1g67720) x ShRk2 (At2g37050)	GK-699C04 2 x SALK_143700	2118
Sec13 (At3g01340) x Nup133 (At2g05120)	SALK_045825C x SALK_092608C	2130
Nup133 (At2g05120)	SALK_092608C	1941
Pollux (At5g49960)	SALK_066135C	2112
ShRk1 Co (At1g67720)	GK-699C04 2 complemented	2089
ShRk2 Co (At2g37050)	SALK_143700 complemented	2079
Sec13 Co (At3g01340)	SALK_045825C complemented	2026
Pollux co (At5g49960)	SALK_066135C complemented	2149

REFERENCES

ALBER, F., DOKUDOVSKAYA, S., VEENHOFF, L. M., ZHANG, W., KIPPER, J., DEVOS, D., SUPRAPTO, A., KARNI-SCHMIDT, O., WILLIAMS, R., CHAIT, B. T., SALI, A. & ROUT, M. P. 2007. The molecular architecture of the nuclear pore complex. *Nature,* 450**,** 695-701.

ANÉ, J., KISS, G., RIELY, B., PENMETSA, R., GILES E. D. OLDROYD, AYAX, C., LÉVY, J., DEBELLÉ, F., BAEK, J.-M., KALO, P., ROSENBERG, C., ROE, B.A., LONG, S.R., DÉNARIÉ, J. & COOK, D. 2004. *Medicago truncatula DMI1* Required for Bacterial and Fungal Symbioses in Legumes. *Science, 303*(5662), 1364-1367.

ANTOLIN-LLOVERA, M., RIED, M. K., BINDER, A. & PARNISKE, M. 2012. Receptor kinase signaling pathways in plant-microbe interactions. *Annu Rev Phytopathol,* 50**,** 451-73.

ANTOLIN-LLOVERA, M., RIED, M. K. & PARNISKE, M. 2014. Cleavage of the SYMBIOSIS RECEPTOR-LIKE KINASE ectodomain promotes complex formation with Nod factor receptor 5. *Curr Biol,* 24**,** 422-7.

ASAI, T., TENA, G., PLOTNIKOVA, J., WILLMANN, M. R., CHIU, W. L., GOMEZ-GOMEZ, L., BOLLER, T., AUSUBEL, F. M. & SHEEN, J. 2002. MAP kinase signalling cascade in *Arabidopsis* innate immunity. *Nature,* 415**,** 977-83.

BANBA, M., GUTJAHR, C., MIYAO, A., HIROCHIKA, H., PASZKOWSKI, U., KOUCHI, H. & IMAIZUMI-ANRAKU, H. 2008. Divergence of Evolutionary Ways Among *Common sym Genes*: *CASTOR* and *CCaMK* Show Functional Conservation Between Two Symbiosis Systems and Constitute the Root of a Common Signaling Pathway, Plant and Cell Physiology, Volume 49, Issue 11, Pages 1659–1671.

BAPTESTE, E., CHARLEBOIS, R. L., MACLEOD, D. & BROCHIER, C. 2005. The two tempos of nuclear pore complex evolution: highly adapting proteins in an ancient frozen structure. *Genome Biol,* 6**,** R85.

BENSMIHEN, S., DE BILLY, F. & GOUGH, C. 2011. Contribution of NFP LysM domains to the recognition of Nod factors during the Medicago truncatula/Sinorhizobium meliloti symbiosis. *PLoS One,* 6**,** e26114.

BINDER, A., LAMBERT, J., MORBITZER, R., POPP, C., OTT, T., LAHAYE, T. & PARNISKE, M. 2014. A modular plasmid assembly kit for multigene expression, gene silencing and silencing rescue in plants. *PLoS One,* 9**,** e88218.

BINDER, A. & PARNISKE, M. 2013a. Analysis of the *Lotus japonicus* nuclear pore NUP107-160 subcomplex reveals pronounced structural plasticity and functional redundancy. *Front Plant Sci,* 4**,** 552.

BINDER, A. & PARNISKE, M. 2013b. The Nuclear Pore Complex in Symbiosis and Pathogen Defence. *Annual Plant Reviews.* John Wiley & Sons Ltd.

BOLLE, C., HUEP, G., KLEINBOLTING, N., HABERER, G., MAYER, K., LEISTER, D. & WEISSHAAR, B. 2013. GABI-DUPLO: a collection of double mutants to overcome genetic redundancy in *Arabidopsis thaliana*. *Plant J,* 75**,** 157-71.

BOWLING, S. A., CLARKE, J. D., LIU, Y., KLESSIG, D. F. & DONG, X. 1997. The *cpr5* mutant of *Arabidopsis* expresses both NPR1-dependent and NPR1-independent resistance. *Plant Cell,* 9**,** 1573-84.

BRAVO, A., YORK, T., PUMPLIN, N., MUELLER, L. A. & HARRISON, M. J. 2016. Genes conserved for arbuscular mycorrhizal symbiosis identified through phylogenomics. *Nat Plants,* 2**,** 15208.

CAILLAUD, M. C., WIRTHMUELLER, L., SKLENAR, J., FINDLAY, K., PIQUEREZ, S. J., JONES, A. M., ROBATZEK, S., JONES, J. D. & FAULKNER, C. 2014. The plasmodesmal protein PDLP1 localises to haustoria-associated membranes during downy mildew infection and regulates callose deposition. *PLoS Pathog,* 10**,** e1004496.

CHARPENTIER, M., BREDEMEIER, R., WANNER, G., TAKEDA, N., SCHLEIFF, E. & PARNISKE, M. 2008. *Lotus japonicus* CASTOR and POLLUX are ion channels essential for perinuclear calcium spiking in legume root endosymbiosis. *Plant Cell,* 20**,** 3467-79.

CHEN, C. W., PANZERI, D., YEH, Y. H., KADOTA, Y., HUANG, P. Y., TAO, C. N., ROUX, M., CHIEN, S. C., CHIN, T. C., CHU, P. W., ZIPFEL, C. & ZIMMERLI, L. 2014. The Arabidopsis malectin-like leucine-rich repeat receptor-like kinase IOS1 associates with the pattern recognition receptors FLS2 and EFR and is critical for priming of pattern-triggered immunity. *Plant Cell,* 26**,** 3201-19.

CHINCHILLA, D., BAUER, Z., REGENASS, M., BOLLER, T. & FELIX, G. 2006. The Arabidopsis receptor kinase FLS2 binds flg22 and determines the specificity of flagellin perception. *Plant Cell,* 18**,** 465-76.

CERRI, M. R., WANG, Q., STOLZ, P., FOLGMANN, J., FRANCES, L., KATZER, K., LI, X., HECKMANN, A. B., WANG, T. L., DOWNIE, J. A., KLINGL, A., DE CARVALHO-NIEBEL, F., XIE, F. & PARNISKE, M. 2017. The *ERN1* transcription factor gene is a target of the CCaMK/CYCLOPS complex and controls rhizobial infection in *Lotus japonicus*. *New Phytol,* 215: 323–337.

CLOUGH, S. J. & BENT, A. F. 1998. Floral dip: a simplified method for *Agrobacterium*-mediated transformation of *Arabidopsis thaliana*. *Plant J,* 16**,** 735-43.

CONSONNI, C., HUMPHRY, M. E., HARTMANN, H. A., LIVAJA, M., DURNER, J., WESTPHAL, L., VOGEL, J., LIPKA, V., KEMMERLING, B., SCHULZE-LEFERT, P., SOMERVILLE, S. C. & PANSTRUGA, R. 2006. Conserved requirement for a plant host cell protein in powdery mildew pathogenesis. *Nat Genet,* 38**,** 716-20.

CURTIS, M. D. & GROSSNIKLAUS, U. 2003. A gateway cloning vector set for high-throughput functional analysis of genes *in planta*. *Plant Physiol,* 133**,** 462-9.

CZECHOWSKI, T., STITT, M., ALTMANN, T., UDVARDI, M. K. & SCHEIBLE, W. R. 2005. Genome-wide identification and testing of superior reference genes for transcript normalization in *Arabidopsis*. *Plant Physiol,* 139**,** 5-17.

DELAUX, P. M., SEJALON-DELMAS, N., BECARD, G. & ANE, J. M. 2013. Evolution of the plant-microbe symbiotic 'toolkit'. *Trends Plant Sci,* 18**,** 298-304.

DELAUX, P. M., VARALA, K., EDGER, P. P., CORUZZI, G. M., PIRES, J. C. & ANE, J. M. 2014. Comparative phylogenomics uncovers the impact of symbiotic associations on host genome evolution. *PLoS Genet,* 10**,** e1004487.

ENDRE, G., KERESZT, A., KEVEI, Z., MIHACEA, S., KALO, P., AND KISS, G.B. 2002. A receptor kinase gene regulating symbiotic nodule development. *Nature,* 417**,** 962–966.

EVANGELISTI, E., REY, T. & SCHORNACK, S. 2014. Cross-interference of plant development and plant-microbe interactions. *Curr Opin Plant Biol,* 20C**,** 118-126.

FAVRE, P., BAPAUME, L., BOSSOLINI, E., DELORENZI, M., FALQUET, L. & REINHARDT, D. 2014. A novel bioinformatics pipeline to discover genes related to arbuscular mycorrhizal symbiosis based on their evolutionary conservation pattern among higher plants. *BMC Plant Biol,* 14**,** 333.

FOX, J. W., S. 2011. An {R} Companion to Applied Regression. Thousand Oaks {CA}: Sage.

GENRE, A., CHABAUD, M., FACCIO, A., BARKER, D. G. & BONFANTE, P. 2008. Prepenetration apparatus assembly precedes and predicts the colonization patterns of arbuscular mycorrhizal fungi within the root cortex of both *Medicago truncatula* and *Daucus carota*. *Plant Cell,* 20**,** 1407-20.

GENRE, A., CHABAUD, M., TIMMERS, T., BONFANTE, P. & BARKER, D. G. 2005. Arbuscular mycorrhizal fungi elicit a novel intracellular apparatus in *Medicago truncatula* root epidermal cells before infection. *Plant Cell,* 17**,** 3489-99.

GHERBI, H., MARKMANN, K., SVISTOONOFF, S., ESTEVAN, J., AUTRAN, D., GICZEY, G., AUGUY, F., PERET, B., LAPLAZE, L., FRANCHE, C., PARNISKE, M. & BOGUSZ, D. 2008. SymRK defines a common genetic basis for plant root endosymbioses with arbuscular mycorrhiza fungi, rhizobia, and Frankiabacteria. *Proc Natl Acad Sci U S A,* 105**,** 4928-32.

GLAZEBROOK, J. 2005. Contrasting mechanisms of defense against biotrophic and necrotrophic pathogens. *Annu Rev Phytopathol,* 43**,** 205-27.

GLAZEBROOK, J., ROGERS, E. E. & AUSUBEL, F. M. 1996. Isolation of *Arabidopsis* mutants with enhanced disease susceptibility by direct screening. *Genetics,* 143**,** 973-82.

GONZALEZ-AGUILERA, C. & ASKJAER, P. 2012. Dissecting the NUP107 complex: multiple components and even more functions. *Nucleus,* 3**,** 340-8.

GRAVES, S., PIEPHO, H. P., SELZER, L. & WITH HELP FROM DORAI-RAJ, S. 2012. multcompView: Visualizations of paired comparisons.

GROTH, M., TAKEDA, N., PERRY, J., UCHIDA, H., DRAXL, S., BRACHMANN, A., SATO, S., TABATA, S., KAWAGUCHI, M., WANG, T. L. & PARNISKE, M. 2010. *NENA,* a *Lotus japonicus* homolog of *Sec13,* is required for rhizodermal infection by arbuscular mycorrhiza fungi and rhizobia but dispensable for cortical endosymbiotic development. *Plant Cell,* 22**,** 2509-26.

GUST, A. A., PRUITT, R. & NÜRNBERGER, T. 2017. Sensing Danger: Key to Activating Plant Immunity. *Trends Plant Sci.,* Volume 22, Issue 9, 779 - 791.

GUTJAHR, C. 2014. Phytohormone signaling in arbuscular mycorhiza development. *Curr Opin Plant Biol,* 20C**,** 26-34.

GUTJAHR, C. & PARNISKE, M. 2013. Cell and developmental biology of arbuscular mycorrhiza symbiosis. *Annu Rev Cell Dev Biol,* 29**,** 593-617.

HARRELL, F. E. J. A. W. C. F. C. D. A. M. O. 2014. Hmisc: Harrell Miscellaneous.

HAYASHI, T., SHIMODA, Y., SATO, S., TABATA, S., IMAIZUMI-ANRAKU, H. & HAYASHI, M. 2014. Rhizobial infection does not require cortical expression of upstream common symbiosis genes responsible for the induction of Ca(2+) spiking. *Plant J,* 77**,** 146-59.

HOK, S., DANCHIN, E. G., ALLASIA, V., PANABIERES, F., ATTARD, A. & KELLER, H. 2011. An *Arabidopsis* (malectin-like) leucine-rich repeat receptor-like kinase contributes to downy mildew disease. *Plant Cell Environ,* 34**,** 1944-57.

HOTHORN, T., BRETZ, F. & WESTFALL, P. 2008. Simultaneous inference in general parametric models. *Biometrical Journal,* 50**,** 346-363.

HÜCKELHOVEN, R. & PANSTRUGA, R. 2011. Cell biology of the plant-powdery mildew interaction. *Curr Opin Plant Biol,* 14**,** 738-46.

IMAIZUMI-ANRAKU, H., TAKEDA, N., CHARPENTIER, M., PERRY, J., MIWA, H., UMEHARA, Y., KOUCHI, H., MURAKAMI, Y., MULDER, L., VICKERS, K., PIKE, J., ALLAN D.J., WANG, T., SATO, S., ASAMIZU, E., TABATA, S., YOSHIKAWA, M., MUROOKA, Y., WU, G.-J., KAWAGUCHI, M., KAWASAKI, S., PARNISKE, M. & HAYASHI, M. 2005. Plastid proteins crucial for symbiotic fungal and bacterial entry into plant roots. *Nature*. 433. 527-31.

JARSCH, I. K., KONRAD, S. S., STRATIL, T. F., URBANUS, S. L., SZYMANSKI, W., BRAUN, P., BRAUN, K. H. & OTT, T. 2014. Plasma Membranes Are Subcompartmentalized into a Plethora of Coexisting and Diverse Microdomains in Arabidopsis and Nicotiana benthamiana. *Plant Cell,* 26**,** 1698-1711.

JONES, J.D.G. & DANGL, J.L. 2006. The plant immune system. *Nature*. volume 444, pages 323–329.

KANAMORI, N., MADSEN, L. H., RADUTOIU, S., FRANTESCU, M., QUISTGAARD, E. M., MIWA, H., DOWNIE, J. A., JAMES, E. K., FELLE, H. H., HAANING, L. L., JENSEN, T. H., SATO, S., NAKAMURA, Y., TABATA, S., SANDAL, N. & STOUGAARD, J. 2006. A nucleoporin is required for induction of Ca^{2+} spiking in legume nodule development and essential for rhizobial and fungal symbiosis. *Proc Natl Acad Sci U S A,* 103**,** 359-64.

KATOH, K., ROZEWICKI, J. & YAMADA, K. D. 2017. MAFFT online service: multiple sequence alignment, interactive sequence choice and visualization, *Briefings in Bioinformatics*, bbx108.

KEMMERLING, B., SCHWEDT, A., RODRIGUEZ, P., MAZZOTTA, S., FRANK, M., QAMAR, S. A., MENGISTE, T., BETSUYAKU, S., PARKER, J. E., MUSSIG, C., THOMMA, B. P., ALBRECHT, C., DE VRIES, S. C., HIRT, H. & NURNBERGER, T. 2007. The BRI1-associated kinase 1, BAK1, has a brassinolide-independent role in plant cell-death control. *Curr Biol,* 17**,** 1116-22.

KEVEI, Z., SERES, A., KERESZT, A., KALO, P., KISS, P., TOTH, G., ENDRE, G. & KISS, G. B. 2005. Significant microsynteny with new evolutionary highlights is detected between *Arabidopsis* and legume model plants despite the lack of macrosynteny. *Mol Genet Genomics,* 274**,** 644-57.

KISTNER, C. & PARNISKE, M. 2002. Evolution of signal transduction in intracellular symbiosis. *Trends Plant Sci,* 7**,** 511-8.

KISTNER, C., WINZER, T., PITZSCHKE, A., MULDER, L., SATO, S., KANEKO, T., TABATA, S., SANDAL, N., STOUGAARD, J., WEBB, K. J., SZCZYGLOWSKI, K. & PARNISKE, M. 2005. Seven *Lotus japonicus* genes required for transcriptional reprogramming of the root during fungal and bacterial symbiosis. *Plant Cell,* 17**,** 2217-29.

KOSUTA, S., HELD, M., HOSSAIN, M. S., MORIERI, G., MACGILLIVARY, A., JOHANSEN, C., ANTOLIN-LLOVERA, M., PARNISKE, M., OLDROYD, G. E., DOWNIE, A. J., KARAS, B. & SZCZYGLOWSKI, K. 2011. Lotus japonicus *symRK-14* uncouples the cortical and epidermal symbiotic program. *Plant J,* 67**,** 929-40.

KURAKU, S., ZMASEK, C. M., NISHIMURA, O.& KATOH, K. 2013. aLeaves facilitates on-demand exploration of metazoan gene family trees on MAFFT sequence alignment server with enhanced interactivity. *Nucleic Acids Research*, Volume 41, Issue W1, Pages W22–W28.

LÉVY, J., BRES, C., GEURTS, R., CHALHOUB, B., KULIKOVA, O., DUC, G., JOURNET, E.-P., ANÉ, J.-M., LAUBER, E., BISSELING, T., DÉNARIÉ, J., ROSENBERG, C. &

DEBELLÉ, F. 2004. A putative Ca2+ and calmodulin-dependent protein kinase required for bacterial and fungal symbioses. *Science*, 303, 1361–1364.

LI, X., CLARKE, J. D., ZHANG, Y. & DONG, X. 2001. Activation of an EDS1-mediated R-gene pathway in the *snc1* mutant leads to constitutive, NPR1-independent pathogen resistance. *Mol Plant Microbe Interact,* 14**,** 1131-9.

LIN, N. C. & MARTIN, G. B. 2005. An avrPto/avrPtoB mutant of *Pseudomonas syringae* pv. *tomato* DC3000 does not elicit Pto-mediated resistance and is less virulent on tomato. *Mol Plant Microbe Interact,* 18**,** 43-51.

MARKMANN, K., GICZEY, G. & PARNISKE, M. 2008. Functional adaptation of a plant receptor-kinase paved the way for the evolution of intracellular root symbioses with bacteria. *PLoS Biol,* 6**,** e68.

MATSUBAYASHI, Y., SHINOHARA, H. & OGAWA, M. 2006. Identification and functional characterization of phytosulfokine receptor using a ligand-based approach. *Chem Rec,* 6**,** 356-64.

MICALI, C., GOLLNER, K., HUMPHRY, M., CONSONNI, C. & PANSTRUGA, R. 2008. The Powdery Mildew Disease of Arabidopsis: A Paradigm for the Interaction between Plants and Biotrophic Fungi. *Arabidopsis Book,* 6**,** e0115.

MIMS, C. W., RODRIGUEZ-LOTHER, C. & RICHARDSON, E. A. 2002. Ultrastructure of the host-pathogen interface in daylily leaves infected by the rust fungus *Puccinia hemerocallidis*. *Protoplasma,* 219**,** 221-6.

MITRA, R.M., GLEASON, C.A., EDWARDS, A., HADFIELD, J., DOWNIE, J.A., OLDROYD, G.E.D. & LONG, S.R. 2004. A Ca2+/calmodulin-dependent protein kinase required for symbiotic nodule development: Gene identification by transcript-based cloning. *Proc. Natl. Acad. Sci. USA*. 101, 4701–4705.

MOFFAT, C. S., INGLE, R. A., WATHUGALA, D. L., SAUNDERS, N. J., KNIGHT, H. & KNIGHT, M. R. 2012. ERF5 and ERF6 Play Redundant Roles as Positive Regulators of JA/Et-Mediated Defense against *Botrytis cinerea* in Arabidopsis. *PLoS ONE*, *7*(4), e35995.

MOSHER, S., SEYBOLD, H., RODRIGUEZ, P., STAHL, M., DAVIES, K. A., DAYARATNE, S., MORILLO, S. A., WIERZBA, M., FAVERY, B., KELLER, H., TAX, F. E. & KEMMERLING, B. 2013. The tyrosine-sulfated peptide receptors PSKR1 and PSY1R modify the immunity of *Arabidopsis* to biotrophic and necrotrophic pathogens in an antagonistic manner. *Plant J,* 73**,** 469-82.

MURASHIGE, T. & SKOOG, F. 1962. A revised medium for rapid growth and bio assays with tobacco tissue cultures. *Physiol Plant,* 15**,** 473-497.

OLDROYD, G. E. 2013. Speak, friend, and enter: signalling systems that promote beneficial symbiotic associations in plants. *Nat Rev Microbiol,* 11**,** 252-63.

ONATE-SANCHEZ, L., ANDERSON, J. P., YOUNG, J. & SINGH, K. B. 2007. AtERF14, a member of the ERF family of transcription factors, plays a nonredundant role in plant defense. *Plant Physiol,* 143**,** 400-9.

PARNISKE, M. 2000. Intracellular accommodation of microbes by plants: a common developmental program for symbiosis and disease? *Curr Opin Plant Biol,* 3**,** 320-8.

PENNINCKX, I. A., EGGERMONT, K., TERRAS, F. R., THOMMA, B. P., DE SAMBLANX, G. W., BUCHALA, A., METRAUX, J. P., MANNERS, J. M. & BROEKAERT, W. F. 1996. Pathogen-induced systemic activation of a plant defensin gene in Arabidopsis follows a salicylic acid-independent pathway. *Plant Cell,* 8**,** 2309-23.

PIMPRIKAR, P., CARBONNEL, S., PARIES, M., KATZER, K., KLINGL, V., BOHMER, M.J., KARL, L., FLOSS, D.S., HARRISON, M.J., PARNISKE, M. & GUTJAHR, C. 2016. A CCaMK-CYCLOPS-DELLA Complex Activates Transcription of *RAM1* to Regulate Arbuscule Branching. *Curr Biol*. Apr 25;26(8):1126.

PUMPLIN, N. & HARRISON, M. J. 2009. Live-cell imaging reveals periarbuscular membrane domains and organelle location in *Medicago truncatula* roots during arbuscular mycorrhizal symbiosis. *Plant Physiol,* 151**,** 809-19.

REY, T., NARS, A., BONHOMME, M., BOTTIN, A., HUGUET, S., BALZERGUE, S., JARDINAUD, M. F., BONO, J. J., CULLIMORE, J., DUMAS, B. et al. 2013. NFP, a LysM protein controlling Nod factor perception, also intervenes in *Medicago truncatula* resistance to pathogens. *New Phytologist* 198: 875–886.

REY, T., CHATTERJEE, A., BUTTAY, M., TOULOTTE, J. & SCHORNACK, S. 2015, *Medicago truncatula* symbiosis mutants affected in the interaction with a biotrophic root pathogen. *New Phytol,* 206: 497–500.

RIED, M. K., ANTOLIN-LLOVERA, M. & PARNISKE, M. 2014. Spontaneous symbiotic reprogramming of plant roots triggered by receptor-like kinases. *Elife,* 3.

RYALS, J. A., NEUENSCHWANDER, U. H., WILLITS, M. G., MOLINA, A., STEINER, H. Y. & HUNT, M. D. 1996. Systemic acquired resistance. *Plant Cell,* 8**,** 1809-1819.

SAITO, K., YOSHIKAWA, M., YANO, K., MIWA, H., UCHIDA, H., ASAMIZU, E., SATO, S., TABATA, S., IMAIZUMI-ANRAKU, H., UMEHARA, Y., KOUCHI, H., MUROOKA, Y., SZCZYGLOWSKI, K., DOWNIE, J. A., PARNISKE, M., HAYASHI, M. & KAWAGUCHI, M. 2007. NUCLEOPORIN85 is required for calcium spiking, fungal and bacterial symbioses, and seed production in *Lotus japonicus*. *Plant Cell,* 19**,** 610-24.

SALVAUDON, L., HÉRAUDET, V. & SHYKOFF J. A. 2008. *Arabidopsis thaliana* and the Robin Hood parasite: a chivalrous oomycete that steals fitness from fecund hosts and benefits the poorest one? *Biol. Lett.* 4 526-529.

SCHOLL, R. L., MAY, S. T. & WARE, D. H. 2000. Seed and molecular resources for *Arabidopsis*. *Plant Physiol,* 124**,** 1477-80.

SHIU, S. H. & BLEECKER, A. B. 2003. Expansion of the receptor-like kinase/Pelle gene family and receptor-like proteins in *Arabidopsis*. *Plant Physiol,* 132**,** 530-43.

SINGH, S., KATZER, K., LAMBERT, J., CERRI, M. & PARNISKE, M. 2014. CYCLOPS, a DNA-binding transcriptional activator, orchestrates symbiotic root nodule development. *Cell Host Microbe,* 15**,** 139-52.

SINGH, S. & PARNISKE, M. 2012. Activation of calcium- and calmodulin-dependent protein kinase (CCaMK), the central regulator of plant root endosymbiosis. *Curr Opin Plant Biol,* 15**,** 444-53.

SLUSARENKO, A. J. & SCHLAICH, N. L. 2003. Downy mildew of *Arabidopsis thaliana* caused by *Hyaloperonospora parasitica* (formerly *Peronospora parasitica*). *Mol Plant Pathol,* 4**,** 159-70.

SOHN, K. H., LEI, R., NEMRI, A. & JONES, J. D. 2007. The downy mildew effector proteins ATR1 and ATR13 promote disease susceptibility in *Arabidopsis thaliana*. *Plant Cell,* 19**,** 4077-90.

SOLANO, R., STEPANOVA, A., CHAO, Q. & ECKER, J. R. 1998. Nuclear events in ethylene signaling: a transcriptional cascade mediated by ETHYLENE-INSENSITIVE3 and ETHYLENE-RESPONSE-FACTOR1. *Genes Dev,* 12**,** 3703-14.

STAMATAKIS, A., HOOVER, P. & ROUGEMONT, J. 2008. A rapid bootstrap algorithm for the RAxML Web servers. *Syst Biol,* 57**,** 758-71.

STRACKE, S., KISTNER, C., YOSHIDA, S., MULDER, L., SATO, S., KANEKO, T., TABATA, S., SANDAL, N., STOUGAARD, J., SZCZYGLOWSKI, K. & PARNISKE, M. 2002. A plant receptor-like kinase required for both bacterial and fungal symbiosis. *Nature,* 417**,** 959-62.

SVISTOONOFF, S., BENABDOUN, F.M., NAMBIAR-VEETIL, M., IMANISHI, L., VAISSAYRE, V., CESARI, S., DIAGNE, N., HOCHER, V., DE BILLY, F., BONNEAU, J., WALL, L., YKHLEF, N., ROSENBERG, C., BOGUSZ, D., FRANCHE, C. & GHERBI, H. 2013. The Independent Acquisition of Plant Root Nitrogen-Fixing Symbiosis in Fabids Recruited the Same Genetic Pathway for Nodule Organogenesis. *PLoS ONE*. 8(5): e64515.

TEAM, R. C. 2013. R: A language and environment for statistical computing. Vienna, Austria: R Foundation for Statistical Computing.

VENKATESHWARAN, M., COSME, A., HAN, L., BANBA, M., SATYSHUR, K. A., SCHLEIFF, E., PARNISKE, M., IMAIZUMI-ANRAKU, H. & ANE, J. M. 2012. The recent evolution of a symbiotic ion channel in the legume family altered ion conductance and improved functionality in calcium signaling. *Plant Cell*, 24**,** 2528-45.

VOEGELE, R. T. & MENDGEN, K. 2003. Rust haustoria: nutrient uptake and beyond. *New Phytologist*. 159: 93–100.

WANG, E., SCHORNACK, S., MARSH, J. F., GOBBATO, E., SCHWESSINGER, B., EASTMOND, P., SCHULTZE, M., KAMOUN, S. & OLDROYD, G. E. 2012. A common signaling process that promotes mycorrhizal and oomycete colonization of plants. *Curr Biol*, 22**,** 2242-6.

WANG, W., WEN, Y., BERKEY, R. & XIAO, S. 2009. Specific Targeting of the Arabidopsis Resistance Protein RPW8.2 to the Interfacial Membrane Encasing the Fungal Haustorium Renders Broad-Spectrum Resistance to Powdery Mildew. *Plant Cell*. 2898–2913.

WIERMER, M., CHENG, Y. T., IMKAMPE, J., LI, M., WANG, D., LIPKA, V. & LI, X. 2012. Putative members of the *Arabidopsis* Nup107-160 nuclear pore sub-complex contribute to pathogen defense. *Plant J*, 70**,** 796-808.

YANO, K., YOSHIDA, S., MÜLLER, J., SINGH, S., BANBA, M., VICKERS, K., MARKMANN, K., WHITE, C., SCHULLER, B., SATO, S., ASAMIZU, E., TABATA, S, MUROOKA, Y., PERRY, J., WANG, T.L., KAWAGUCHI, M., IMAIZUMI-ANRAKU, H., HAYASHI, M. & PARNISKE, M. 2008. CYCLOPS, a mediator of symbiotic intracellular accommodation. Proc. Natl. Acad. Sci. USA. 105 (51) 20540-20545.

ZHANG, Y. & LI, X. 2005. A putative nucleoporin 96 Is required for both basal defense and constitutive resistance responses mediated by suppressor of npr1-1,constitutive 1. *Plant Cell*, 17**,** 1306-16.